Sensitivity of African Easterly Waves to Dust Forcing

Hamza Kunhu Bangalath[1], Jerry Raj[1], and Georgiy Stenchikov[1]

[1]Physical Science and Engineering Division, King Abdullah University of Science and Technology, Thuwal, Saudi Arabia

Key Points:

- African easterly waves are highly sensitive to dust shortwave absorption.
- Wave track intensifies, broadens, and shifts southward in response to dust shortwave absorption
- AEW sensitivity to dust stems primarily from baroclinic and barotropic energy conversions and energy generation by adiabatic heating.

Corresponding author: Hamza Kunhu Bangalath, hamzakunhu.bangalath@kaust.edu.sa

Abstract

[There is a lack of agreement on the sign and magnitude of the effect of dust-radiative forcing on African easterly waves (AEWs) among past studies. The uncertainty in the dust-radiative forcing associated with the estimation of shortwave absorption is a leading cause of disagreement in the literature. The inability of models to represent various dust–AEW interaction pathways also leads to uncertainty among modeling studies. The present study investigates the sensitivity of AEWs to the observed variability in dust shortwave absorption using a high-resolution atmospheric general circulation model. Global simulations are conducted at a spatial resolution of about 25 km to simulate AEWs and associated circulation features adequately well. The results reveal that AEWs are highly sensitive to dust shortwave absorption. In addition, the AEW activity intensifies and broadens the wave track with a southward shift in response to dust shortwave absorption. There is approximately a 25 % change in eddy kinetic energy (EKE) associated with AEWs for the range of dust shortwave absorption used. The 6-9–day waves are more sensitive to dust shortwave absorption than the 3-5–day waves, where the response in the former has a stark land–sea contrast. The sensitivity of AEW to dust heating stems from a combination of the response from various energy conversions. Although baroclinic energy conversion is the leading term in the energy cycle, the responses to dust shortwave heating in barotropic and generation terms are comparable to those in baroclinic conversion.]

Plain Language Summary

African easterly waves (AEWs) occur in the dust-laden atmosphere over tropical Africa and the Atlantic. Dust and AEWs interact with each other in multiple ways. However, there has yet to be a general agreement on the sign and magnitude of dust effect on the AEWs. A primary uncertainty comes from estimating dust's ability to absorb shortwave radiation and heat the atmosphere. This study investigates the sensitivity of AEWs to the observed variability in dust shortwave absorption using a high-resolution atmospheric general circulation model. The results demonstrate that AEWs are highly sensitive to dust shortwave absorption. The AEW activity intensifies and broadens the wave track as the dust becomes more absorbing. Wave track widens primarily towards the equator, leading to a southward track shift. There is approximately a 25 % change in the eddy kinetic energy, a proxy for AEW activities, for the observed range of dust shortwave absorption. Hence, accurately representing dust optical properties is crucial to predict the AEWs and the overall African climate better, especially in the global warming context where both AEWs and dust loading change.

1 Introduction

Heavy loading of mineral dust aerosols and African easterly waves (AEWs) co-exist in the Sahara–Sahel–tropical Atlantic region. The interaction between AEWs and dust-radiative forcing has been the subject of active scientific inquiry since the 1970s (e.g., Carlson & Prospero, 1972). Although a vast body of modeling and observational studies have been conducted on dust–AEW interaction to date, no general agreement has been reached on the effect of dust on AEWs. Some studies have demonstrated the enhancement of AEW activities as a response to dust-radiative forcing (e.g., Karyampudi & Carlson, 1988; Reale et al., 2009; Jury & Santiago, 2010), whereas other studies have suggested the weakening of AEWs due to dust forcing (e.g., Jones et al., 2004; Ma et al., 2012; Grogan et al., 2016; Lavaysse et al., 2011). The disagreement among studies stems primarily from the uncertainties in estimating dust-radiative forcing and from the inability of models to incorporate all possible dust–AEW interaction pathways adequately.

One of the main uncertainties in estimating dust-radiative forcing lies in the estimation of dust shortwave absorption and its associated radiative heating (e.g., Solmon et al., 2008; Miller et al., 2004). Balkanski et al. (2007) found that the imaginary part

of the refractive index, which decides the dust shortwave absorption and radiative heating rate, varies by an order of magnitude among various studies. Accordingly, single scattering albedo, the ratio of scattering and absorption in the total extinction, varies significantly (0.7 to 0.99) (e.g., J. M. Haywood et al., 2001; Slingo et al., 2006; Otto et al., 2009; Raut & Chazette, 2008). There is also a disparity between in situ and satellite measurements; in situ measurements generally lead to a higher shortwave absorption estimation than satellite-based estimates (e.g., Kaufman et al., 2001; J. Haywood et al., 2003). Hence, modeling studies struggle with the uncertainty of radiative forcing estimation.

Changes in dust shortwave absorption can affect the generation and maintenance of AEWs in many ways. Many previous studies have demonstrated that dust-induced radiative heating in the lower and mid-troposphere alters the static stability of the atmosphere, influencing the AEWs (e.g., Jones et al., 2004). Another vital pathway of dust–AEW interaction is through the instabilities of the African easterly jet (AEJ). The dust-induced changes in the shear on the AEJ and the consequent barotropic-baroclinic instabilities are necessary to maintain the AEW (e.g., Thorncroft & Hoskins, 1994a, 1994b; Hall et al., 2006; Cornforth et al., 2009). However, more recent studies (Grogan et al., 2016, 2017; Nathan et al., 2017; Bercos-Hickey et al., 2017) have revealed that changes in the dust-induced zonal mean and eddy heating can also influence AEWs.

Bangalath and Stenchikov (2016) studied the sensitivity of the Middle East and North African (MENA) climate to the uncertainty in dust shortwave absorption. The study found that dust acts as an off-equatorial heating source collocated with the solar insolation maximum and enhances the meridional mean temperature gradient over the MENA region during summer. The tropical rain-belt, surface circulation (trade winds), and AEJ intensify and shift northward as dust shortwave absorption increases. The sensitivity of the tropical rain-belt and AEJ to dust shortwave absorption indeed translates into AEW sensitivity because the generation and maintenance of AEWs greatly depend on the moist convection and instabilities of AEJ. The tropical rainbelt shifts northward and intensifies as a response to dust heating. The latent heat release from the enhanced precipitation alters the meridional temperature gradient in the mid-upper troposphere. The circulation responses at the surface and at the level of the AEJ are particularly crucial for AEWs. The surface circulation south of the inter-tropical depression (monsoonal trade wind) enhances, and the circulation north of it (Harmattan wind) weakens due to dust shortwave heating. In contrast, circulation weakens on the southern flank of the AEJ and enhances on its northern flank. The contrasting response pattern in surface and mid-tropospheric circulation induces vertical shear in the zonal and meridional velocities. Perturbations in wind shear and temperature gradients change all energy conversion terms in the regional energy cycle, ultimately changing the eddy kinetic energy (EKE) available for AEWs (e.g., Grogan et al., 2016, 2017; Nathan et al., 2017; Bercos-Hickey et al., 2017).

The present study investigates the sensitivity of AEWs to the observed variability in dust shortwave absorption using a high-resolution atmospheric general circulation model-HiRAM-developed at the Geophysical Fluid Dynamics Laboratory (GFDL) (Zhao et al., 2009). In order to quantify the sensitivity, the study conducts climate simulations with seasonally varying dust assuming dust is an inefficient, standard, and efficient shortwave absorber, following Bangalath and Stenchikov (2016). Apart from quantifying the sensitivity of AEWs to dust shortwave absorption, this research specifically investigates the causality of sensitivity using energetics analysis. The study analyzes the response of 3-5–day and 6-9–day wave sensitivity separately over continental Africa and the Atlantic. The HiRAM simulations are conducted at a spatial resolution of 25 km. It is worth noting that most past AEW modeling studies have used coarse-resolution general circulation models (GCMs), which often fail to resolve the topography and mesoscale systems well enough to produce realistic AEWs. The HiRAM simulations at 25 km have been proven to resolve AEWs adequately (Raj et al., 2022). This study specifically ap-

plies energetic analysis to understand the sensitivity of AEWs to dust shortwave absorption.

2 Model and Experiment

HiRAM was developed from the Atmospheric Model version 2 (AM2) of GFDL by modifying certain aspects (Zhao et al., 2009), which has flexibility in the horizontal resolution of up to a few kilometers and improved vertical resolution (32 levels) compared to AM2. The current study uses the C360 version (spatial resolution of about 25km) of the HiRAM, which employs a hydrostatic finite-volume cubed-sphere dynamical core (Lin 2004; Putman and Lin 2007). A major modification from AM2 is that its customary deep convective scheme is replaced by a nonintrusive shallow convective scheme (Bretherton et al. 2004) by extending it to simulate deep convection (Zhao et al. 2009). Moreover, HiRAM preserves most of the parameterizations from AM2, such as radiative transfer, surface flux, boundary layer, orographic gravity wave drag parameterizations, and large-scale cloud microphysics, with necessary modifications as the resolution increases. Further, HiRAM is coupled to GFDL land model LM3, and sea surface temperature (SST) is prescribed from the monthly Hadley Centre Sea Ice and Sea Surface Temperature (HadISST) dataset (Rayner et al., 2003). It should be noted that the simulations do not account for the SST feedback to dust loading, and the response to dust is solely from the atmospheric response.

Originally HiRAM was designed to provide an improved representation of weather events in a GCM and for applications ranging from weekly forecasts to climate projections. A resolution of 25km allows models to resolve important mesoscale weather events (e.g., Zhao et al., 2009; Jung et al., 2012) and major orographically induced circulations (e.g., Boyle & Klein, 2010; Lau & Ploshay, 2009). Therefore, the simulations enable the examination of sub-seasonal (synoptic scale) variability such as AEWs. A detailed validation of HiRAM's ability to reasonably simulate AEW activities has been reported by Raj et al. (2022). In general, HiRAM simulates EKE reasonably well for both 3-5–day and 6-9–day waves compared to different reanalysis data. It has also been shown that the model is capable of simulating all major circulation features and various energy conversions that make up available potential energy for eddies.

We conducted four experiments: one without dust loading ("NoDUST" experiment) and three with seasonally varying dust loading but with different dust optical properties. The dust and other aerosol concentrations were prescribed from the Model for Ozone and Related Chemical Tracers (MOZART) offline calculations (Horowitz et al. 2003). Dust loading is discretized into eight bins from 0.1 to 10 μm. Specific extinction coefficients of dust are calculated using the Mie theory, assuming refractive indices for the shortwave spectrum from the estimates by Balkanski et al. (2007) and indices for the longwave spectrum by Volz (1973). Three cases of dust with a hematite content (by volume) of 0.9%, 1.5%, and 2.7% were selected. The cases of 0.9% of hematite ("DUST0.9" experiment), 1.5% of hematite ("DUST1.5" experiment), and 2.7% of hematite ("DUST0.9" experiment) represent dust as an inefficient, standard and efficient shortwave absorber, respectively. A detailed explanation of the model and dust representation is presented in Bangalath and Stenchikov (2016).

The sensitivity of AEWs to dust shortwave absorption and the associated heating is estimated by comparing the three dust simulations with simulations without dust. All four experiments were run for an 11-year period with three ensembles (perturbed initial condition runs), and the first year is omitted from the analysis considering the spin-up period.

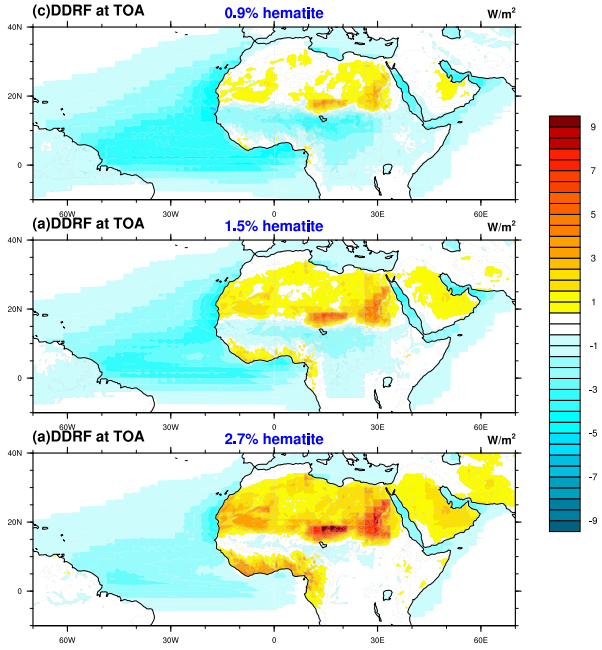

Figure 1. Summer (June–September) all-sky DDRF (Wm^2) at the TOA in the DUST0.9, DUST1.5, and DUST2.7 experiments. Positive values represent the warming of the system, and negative values denote the cooling of the system, by definition

3 Results

3.1 Dust-Radiative Forcing and Atmospheric Heating

Instantaneous radiative forcing and heating rate anomalies were calculated following (Bangalath & Stenchikov, 2015, 2016) in each simulation for analyzing the direct radiative effect of dust. Dust direct radiative forcing (DDRF) is defined as the net (longwave plus shortwave) radiative flux difference between a state with dust loading and one without dust loading (downwelling minus upwelling), calculated under the same meteorological conditions. Hence, positive (negative) DDRF indicates the warming (cooling) of a system. The radiative fluxes of dust were estimated at each radiation time-step by calling the radiation routine twice, with and without the presence of dust. The DDRF and dust-induced atmospheric heating estimates in the present study are calculated under all-sky conditions. A detailed discussion of the dust-radiative forcing and heating rates is available in Bangalath and Stenchikov (2016).

The present study focuses on June–September, the AEW season. The analysis was separately performed over the African continent and the Atlantic. Figure 1 illustrates the top of the atmosphere (TOA) DDRF over MENA and the Atlantic region in all three cases of hematite content. There is a strong north–south gradient in forcing over MENA; the forcing is positive over Saharan-Arabian deserts and negative over sub-Saharan and Oceanic regions. The change in the sign of forcing between bright deserts and relatively dark surfaces, including vegetated canopy and oceans, is due to the albedo effect (e.g., Bangalath & Stenchikov, 2015; Osipov et al., 2015). The TOA aerosol forcing is a strong function of the effective albedo of the underlying surface. As dust becomes more absorbing, the positive forcing over the desert region intensifies, and the negative forcing over the ocean and sub-Saharan region diminishes. The variability of forcing over the Sahel is especially interesting. The forcing changes sign from negative to positive as the dust

becomes more absorbing. As a result, dust-radiative forcing becomes larger over land than over the ocean when the dust becomes more absorbing.

The presence of the north–south gradient in forcing over the African continent is particularly important for AEW activity. Such a north–south contrast in radiative forcing and its strengthening in response to dust shortwave absorption leads to the strengthening and northward shift of the Hadley Cell, rainbelt, and AEJ (Bangalath & Stenchikov, 2015, 2016). The generation and maintenance of AEW greatly depend on the barotropic-baroclinic instabilities; thus, the dust-induced changes in the latent heating and wind shears will affect AEW. To explicitly demonstrate these processes, we separately display the meridional cross sections of zonally averaged dust-induced heating rate anomalies over the continent and Atlantic (Fig. 2). Heating from dust shortwave absorption is confined to the northern hemispheric subtropics centered at 20^0N in all three experiments. Dust-induced heating is concentrated north of the AEJ core (12^0N), which has implications for AEW growth (Grogan et al., 2016, 2017; Grogan & Thorncroft, 2019). As the hematite content increases, the heating increases and broadens meridionally and vertically. Over the Atlantic, the intensity and vertical extent of heating are almost half of those over the continent. Hence, dust forcing affects AEWs over the continent and ocean differently.

3.2 AEW Response

The EKE is a suitable metric to portray wave activity and is calculated as follows:

$$EKE = \frac{(u'^2 + v'^2)}{2} \tag{1}$$

where u and v are the zonal and meridional winds, respectively. The primes indicate Butterworth bandpass-filtered anomalies of the daily wind field. Figure 3 depicts the filtered EKE (for 3-5–day and 6-9–day bands) at 700 hPa (contours) as a measure of AEW activities and displays the difference in filtered EKE (shades) between simulations with and without dust. The differences are taken by subtracting the case with dust from that without dust such that the anomalies express the role of dust in the EKE. The areas where the effect of the dust is statistically significant at a 95% confidence level are marked by dots. The green contours represent the EKE in simulations with dust, and the violet contours represent the EKE in simulations without dust. The EKE is separately estimated for the 3-5–day and the 6-9–day waves. Raj et al. (2022) validated the HiRAM-produced EKE in detail.

In general, dust shortwave heating increases 3-5–day EKE, indicating increased AEW activities (Fig. 3, left column). In the DUST0.9 and DUST1.5 experiments, a north–south EKE dipole pattern occurs in response. Dust causes the weakening of the 3-5–day waves on the northern side of the wave track and enhances on the southern side. A comparison of filtered EKE contours of the DUST (green) and NoDUST (violet) experiments indicates a southward shift of the AEW track in both cases. The dipole response pattern and the southward track shift are more prominent in the DUST0.9 case. The dipole pattern of response disappears as the dust becomes an efficient shortwave absorber (DUST2.7). In this case, the 3-5–day wave activity intensifies everywhere, and the wave track broadens in all directions. Note that the AEW track extends about 450 km in the Atlantic. The broadening and intensification of the AEW track may have implications on the TC genesis in the basin as AEWs are often precursors to tropical cyclones(e.g., Landsea, 1993; Russell et al., 2017). However, care must be taken in drawing a direct correlation between the AEWs and tropical cyclone activities, as a recent study by Patricola et al. (2018) has pointed out that the AEWs may not be a reliable predictor for the seasonal variability and changes in Atlantic tropical cyclone frequency.

In contrast with 3-5–day waves, a striking land–sea contrast occurs in the 6-9–day waves (Fig. 3, right column). Over the land, the wave activity reduces in all three dust

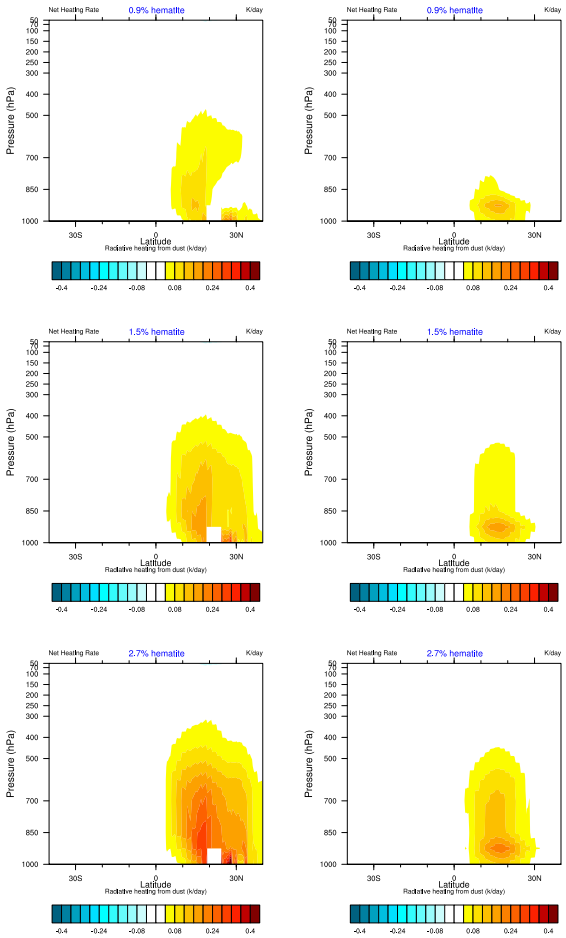

Figure 2. Meridional height cross-section of mean June–September radiative heating rate (shortwave plus longwave) anomaly induced by dust in all three with dust experiments. The left panel represents the vertical cross-section over the African continent (zonally averaged between -15^0 and 20^0), and the right panel is the cross-section for the Atlantic (zonally averaged between -50^0 and -15^0)

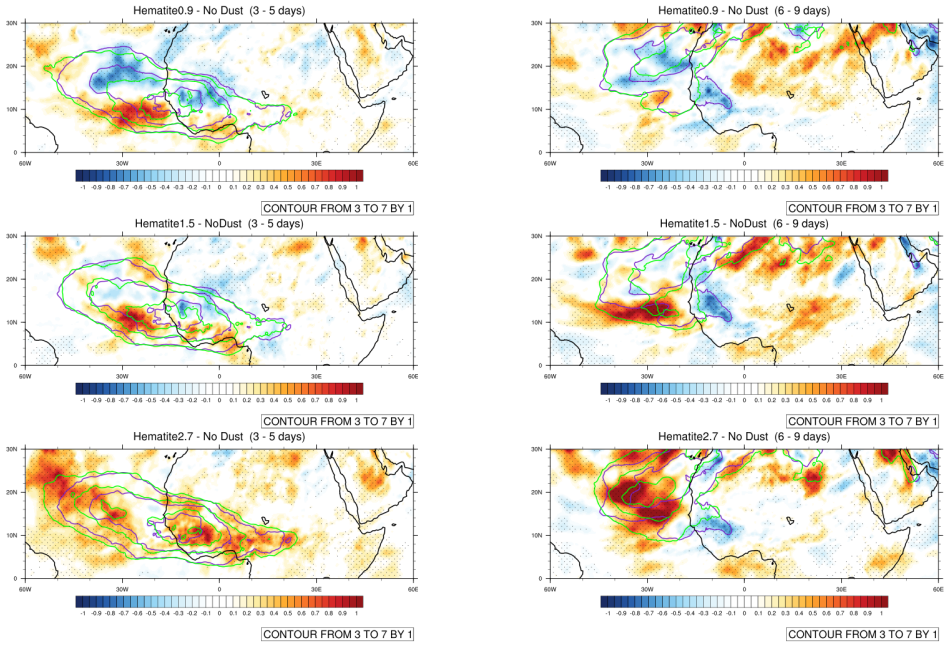

Figure 3. The EKE ($m^2 s^{-2}$) estimated from the 3-5–day band-pass-filtered zonal and meridional winds at 700 hPa. The contours represent the EKE from NoDUST (violet) and three different DUST (green) experiments. Red and blue shades mark the anomalies of EKE in each experiment (DUST-NoDUST). Dots mark areas where the EKE anomalies are statistically significant, at least at the 95% confidence level.

experiments. In addition, the wave track shrinks over land. However, the response over the Atlantic is similar to that of the 3-5–day waves. In the DUST0.9 case, AEW activity decreases in most areas except a few patches to the southern edge of the track. However, a dipole pattern emerges in the DUST1.5 experiment. A southward shift of the 6-9–day wave track is also evident in the DUST1.5 case. Similar to the 3-5–day case, there is an intense and widespread increase in the wave activity and the consequent broadening of wave track in all directions when the dust is highly absorbing (DUST2.7). Such a strong response leads to a strong land–sea contrast in the response. If we assume all individual waves originated over the continent, the strong land–sea contrast in the response indicates an enhancement of AEWs once they enter the Atlantic. The magnitude of response is higher in the 6-9–day waves than in the 3-5–day waves, although the mean EKE of the 3-5–day waves is higher. Therefore, amplified EKE response occurs in the 6-9–day waves compared to the 3-5–day waves, especially in terms of the percentage of change in EKE.

Standard deviations of band-pass-filtered outgoing longwave radiation (OLR) anomalies in 3-5–day and 6-9–day bands are depicted to elucidate the sensitivity of convective activities associated with AEW (Fig. 4). The contours represent the band-pass-filtered variability of OLR in the NoDUST case. The OLR variability is mostly concentrated over tropical Africa and the Atlantic. Over the continent, the OLR variability is collocated with the AEW track defined by the EKE. However, there is a southward shift of the Atlantic AEW track defined by the OLR compared to that defined by the EKE. In other words, the convective activity associated with AEWs is confined to the equator, whereas the wind variability shifts further north in the Atlantic than over the continent. Such a land–sea contrast might be due to the ITCZ's relatively weaker seasonal (latitudinal) oscillation over the Atlantic compared to that over continental Africa.

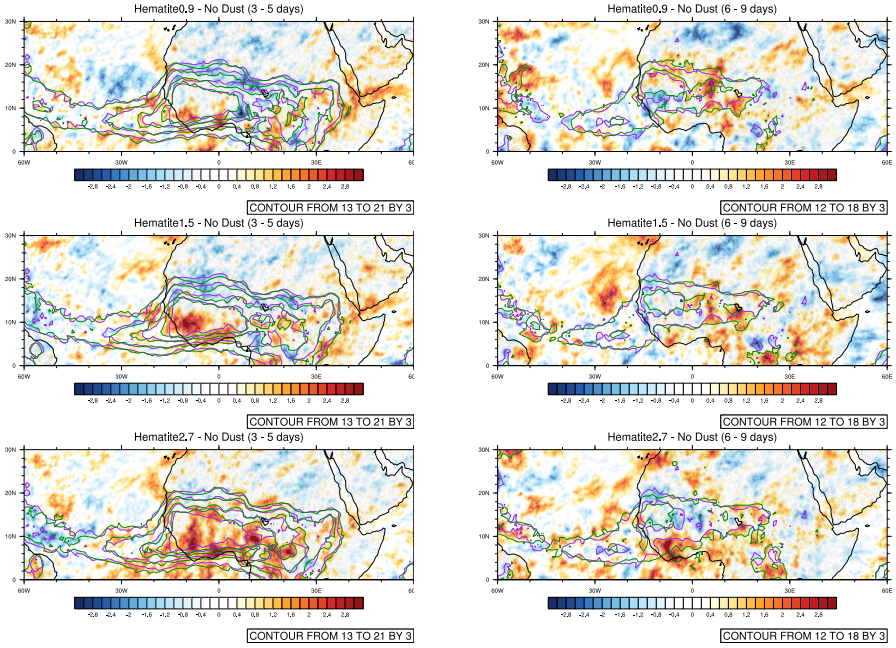

Figure 4. Difference in the 3-5–day band-pass-filtered OLR (wm^{-2}) standard deviation (shading) between experiments with and without dust (DUST-NoDUST). The contours represent the standard deviation of the OLR in the experiment without dust (NoDUST).

Consistent with the response in the EKE field, a north–south dipole pattern occurs in the OLR variability response in the DUST0.9 and DUST1.5 cases. The OLR variability decreases to the north and increases to the south of the AEW track. There is a widespread increase in the OLR variability throughout the track in highly absorbing dust cases (DUST2.7 case), similar to the EKE response. In the 6-9–day case, OLR variability is reduced in most of the track over land. However, the OLR variability to the south of the track intensifies as the dust becomes more absorbing. This is consistent with the response in EKE, and it reaffirms the southward shift of the track response to dust shortwave heating. Over the Atlantic, the OLR variability reduces in the core of the track. However, the variability of OLR increases around the track in all directions indicating the broadening of the track with a dust shortwave absorption increase.

3.3 Energetics Analysis

Energetic analysis is an excellent tool for understanding the generation and maintenance of AEWs (e.g., Norquist et al., 1977; Hsieh & Cook, 2007). This analysis has also been used to assess the influence of dust-radiative forcing on AEWs (Bercos-Hickey et al., 2022; Grogan et al., 2016; Grogan & Thorncroft, 2019). Here, we employed the energetics analyses originally formulated by Lorenz (1955) for the general circulation of the atmosphere and later modified for a limited area (Muench, 1965; Norquist et al., 1977; Hsieh & Cook, 2007) by incorporating energy transport at the boundaries. In this formulation, the governing equations for the EKE (K_E) and available potential energy (A_E) are as follows:

$$\frac{\partial K_E}{\partial t} = C_k + C_{pk} - D_E + K_{EB} + \phi_{EB} \tag{2}$$

and

$$\frac{\partial A_E}{\partial t} = C_A - C_{pk} + G_E + A_{EB} \tag{3}$$

In Equation 2, C_k is the barotropic energy conversion term estimating the conversion of zonal kinetic energy to EKE associated with zonal (u) and meridional (v) wind shears. The C_{pk} is the baroclinic energy conversion term which represents the conversion of eddy available potential energy to EKE associated with the vertical overturning. The C_{pk} appears in Equation 3 with a negative sign indicating that the A_E consumed by baroclinic overturning is converted to K_E. The D_E is the frictional dissipation, and K_{EB} and ϕ_{EB} are boundary EKE flux and pressure work done by the eddies at the boundaries, respectively. The conversion of zonal A_E to eddy A_E from the eddy heat flux along mean zonal temperature gradient is represented by the C_A in Equation 3. The G_E estimates the A_E generation by diabatic heating, either by heating the warmer region and cooling the colder region or by heating the colder region and cooling the warmer region at the same latitude. Finally, A_E fluxes at the boundaries are indicated by A_{EB}. Detailed expressions of all individual terms are provided in Appendix A.

We analyzed the baroclinic (C_{pk}), barotropic (C_k), zonal to eddy potential temperature conversion (C_A), and generation term (G_E) for both 3-5 and 6-9–day waves separately. Dust-radiative forcing changes its sign from land to the ocean (Fig. 1); therefore, we also computed each term separately over the continent (averaged over 15^0W to 20^0E) and Atlantic (averaged over 50^0W to $15^0$0W).

Figure 5 presents C_{pk}, which is the most prominent term, over the continent for the 3-5–day and 6-9–day waves. There are two centers with a positive value (generation center) of C_{pk}: one in the subtropical (12^0N - 30^0N) lower troposphere (from surface to 700 hPa), and the second in the tropical (0^0 - 15^0N) upper troposphere (from 500 hPa to 200 hPa). The former is associated with either the warm air ascent (dry convection) or cold air subsidence, mostly coincident with the Saharan heat-low region. The latter, which is in the upper troposphere, is associated with the latent heat released from the precipitation induced by AEWs. A region of energy destruction also occurs below 500 hPa in the tropics, although the values are at least one order less than the generation center in the upper troposphere. This region of negative C_{pk} is associated with ascending cold air, possibly due to the dynamical forcing within the waves (Yanai, 1961; Diedhiou et al., 2002; Hsieh & Cook, 2007). As baroclinic energy conversion is associated with the overturning circulation, the centers can be understood as part of the tropical deep and moist overturning circulation and the subtropical dry convection.

In the 3-5–day wave (left column), C_{pk} increases in the tropical upper tropospheric generation center as dust shortwave absorption increases. There is approximately 20% increase in the DUST2.7 case compared to NoDUST. The increase in C_{pk} in response to the increase in shortwave heating is due to the enhanced latent heat release from the wave-induced precipitation enhancement. In the subtropical lower tropospheric positive maxima, C_{pk} is destroyed in the DUST0.9 and DUST1.5 cases compared to the NoDUST case. However, intense C_{pk} generation occurs when the dust is an efficient shortwave absorber (DUST2.7). In the remaining area, the C_{pk} response is minimal.

In the 6-9–day wave (right panel Figure 5), C_{pk} is weaker compared to the 3-5–day case due to the lesser convective precipitation associated with 6-9–day waves compared to 3-5–day waves. The 6-9–day C_{pk} values are about half of those in the 3-5–day cases. The C_{pk} patterns are similar in both cases. However, the response to dust shortwave absorption is more significant in the 6-9–day waves than in the 3-5–day waves with a strong north–south dipole pattern, especially in the tropical upper tropospheric center. In addition, C_{pk} is generated towards the equator and destroyed towards the subtropics. The dipole pattern of response enhances when dust-induced shortwave heating increases. Such a dipole pattern of response may be related to the southward shift of 6-9–day AEWs (Fig.

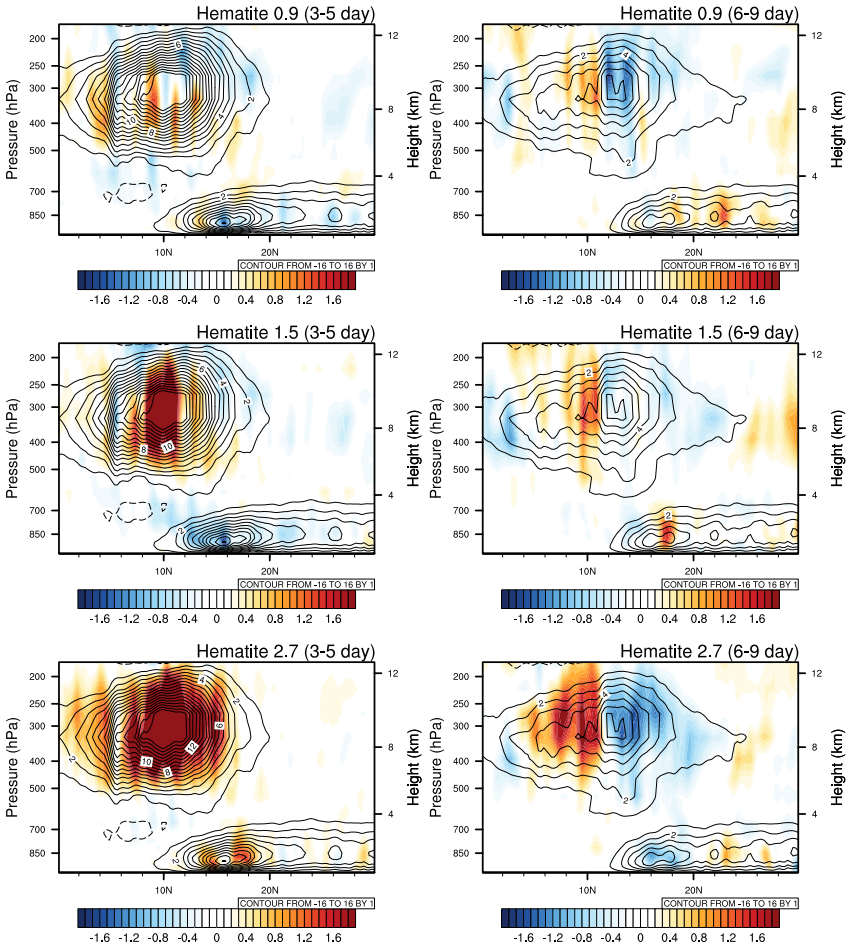

Figure 5. Meridional height cross-sections of the baroclinic energy conversion term (C_{pk}) averaged (15^0 W to 20^0 E) over the continental region. Contours represent the values of C_{pk} in the "NoDUST" simulation, and the shaded contours represent anomalies (DUST-NoDUST) in all three dust experiments.

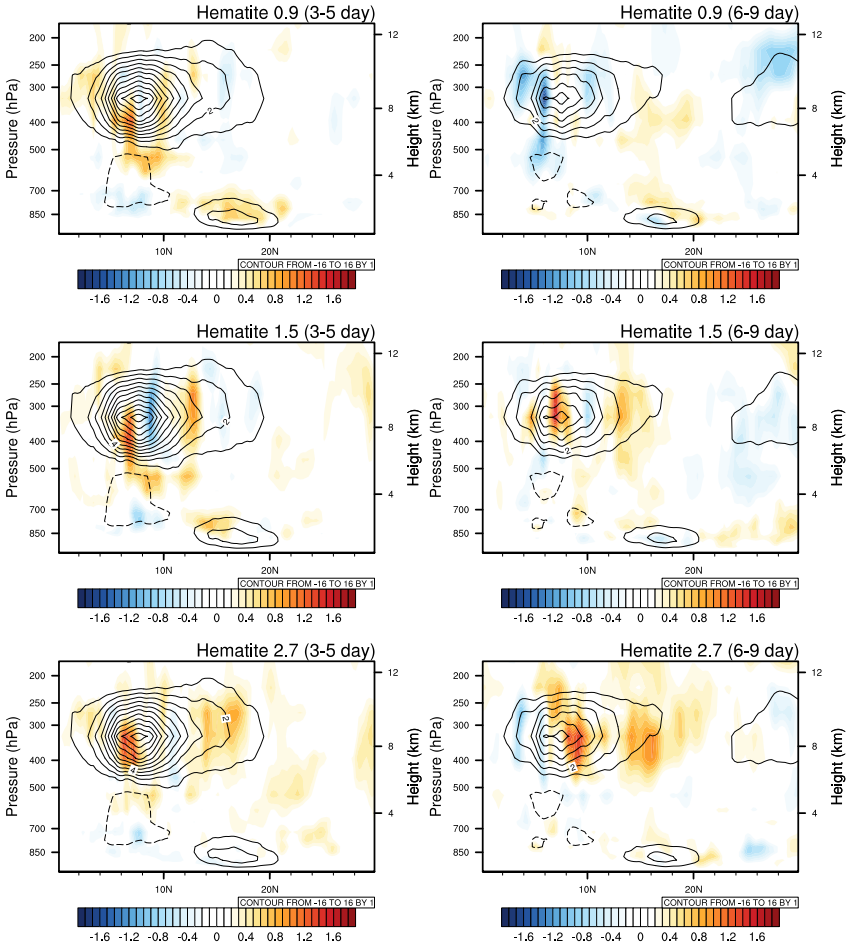

Figure 6. Same as Fig. 5, but averaged (50^0 W to 15^0 W) over the Atlantic.

3) as a response to shortwave heating. On either side of the tropical upper tropospheric center, the relative change (with respect to the NoDUST case) in C_{pk} is about 70% in the DUST2.7 case. Therefore, the relative change in C_{pk} is much higher in the 6-9–day waves than in the 3-5–day waves. The response in the subtropical lower tropospheric generation center also shifts, i.e., it exhibits a dipole response pattern, although the anomalies are weaker. Additionally, C_{pk} decreases on the southern extent of the subtropics, whereas C_{pk} is generated to the north. The dipole pattern enhances and shifts as dust heating increases.

In the Atlantic (Fig. 6), the baroclinic generation of the EKE associated with both 3-5–day and 6-9–day waves is weak compared to the continental area because the waves start to weaken as they pass through the Atlantic. As in the continental case, C_{pk} is weaker in the 6-9–day waves compared to the 3-5–day waves. The Atlantic 3-5–day case response is weaker than its continental counterpart, though there is a stronger increase (more than 50% increase in the DUST2.7 case) in C_{pk} to the northern edge of its upper tropospheric maxima. Unlike the continental case, the subtropical lower tropospheric maxima reveal an increase in the DUST0.9 case, and the response weakens as shortwave absorption increases. The dipole response pattern in the 6-9–day case is relatively less defined over the Atlantic than over land. Instead, widespread energy dissipation occurs in the upper troposphere in the DUST0.9 case, whereas the DUST1.5 and DUST2.7 cases primarily exhibit energy generation, especially on the northern side. The relative change in C_{pk} to the north of the upper tropospheric maxima is about 70% in the high-absorbing dust case (DUST2.7).

Figure 7 presents C_k, which is the next most significant EKE-producing term after C_{pk}, over the continent for the 3-5 and 6-9–day waves. There are three energy production (positive centers) regions. The first is in the deep tropics tropopause (around 200 hPa) associated with the wind shear in the TEJ. The second is in the tropical (centered at 10^0N) mid-troposphere (850 hPa - 300 hPa) associated with the wind shear in the AEJ. The third is in the subtropical (15^0N - 25^0N) lower troposphere (below 850 hPa) associated with Saharan heat low where trade wind meets the dry Harmattan winds (see figure 11 Bangalath and Stenchikov (2016)). It has to be noted that the positive barotropic energy conversion occurs on the equator side of the AEJ (the jet core is at 12^0 lat). The C_k is close to zero or negative on the poleward flank of the AEJ. In other words, barotropic energy conversion that maintains AEWs primarily occurs to the south of the AEJ, where mostly 3-5–day waves happen. On the northern side of the jet, C_k is either small or consumed. However, a strong production of C_k occurs below AEJ to the north of the jet core associated with the Saharan heat low, where trade winds converge in summer. A large region of EKE sink (negative C_k) towards the north extends from 850 hPa to the tropopause, with the center near the tropopause. This sink is associated with the shear in the subtropical jet.

In the 3-5–day waves (Fig. 7 left column), the generation of the EKE from the C_k associated with the wind shear in the equatorward flank of AEJ has an intense response to dust shortwave absorption. In the DUST0.9 case, the EKE dissipates in this region, whereas the EKE is generated in favor of the AEW as the dust shortwave absorption increases (DUST0.9 and DUST2.7 cases). In addition, C_k changes more than 50% between DUST0.9 and DUST2.7 cases on the southern side of the AEJ. In the subtropical generation center in the lower troposphere, C_k is generated and increases with dust-induced heating. However, the maximum response is observed near the tropopause collocated with the TEJ and STJ. As the dust shortwave absorption increases, C_k reduces in this region. The changes in the STJ and TEJ might be caused by AEW modulations or be forced by the dust-radiative forcing. However, disentangling these two possible effects and their interactions with AEW is beyond the scope of the present paper.

In the 6-9–day waves (Fig. 7 left column), C_k over the AEJ location is relatively weaker compared to the 3-5–day waves. The magnitude of response to the dust short-

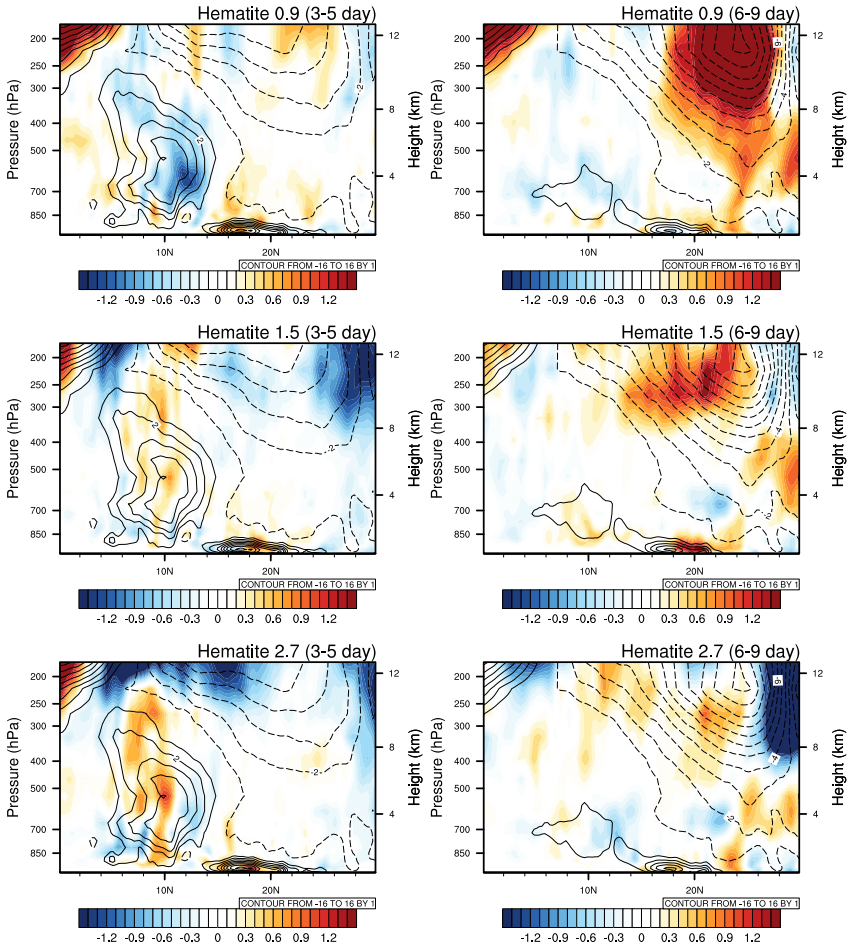

Figure 7. Meridional height cross-sections of the barotropic energy conversion term (C_k) averaged (15^0 W to 20^0 E) over the continental region. Contours represent the values of C_k in the "NoDUST" simulation, and the shaded contours represent anomalies (DUST-NoDUST) in all three dust experiments.

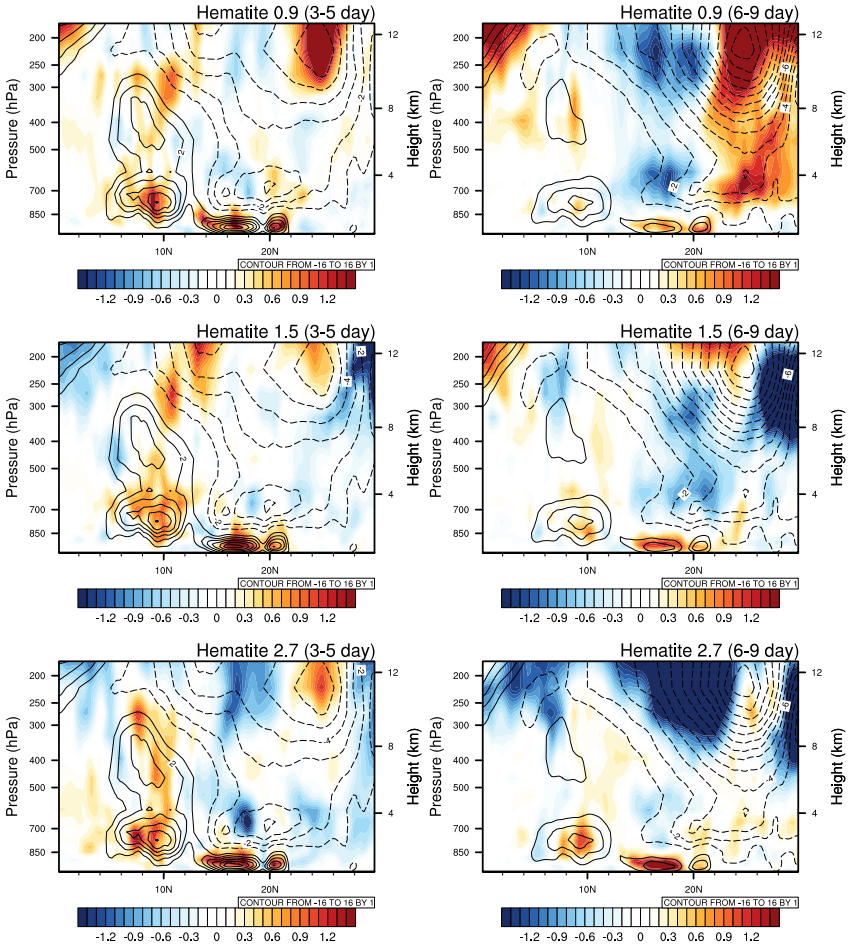

Figure 8. Same as Fig. 7, but averaged (50^0 W to 15^0 W) over the Atlantic.

wave absorption is also small, although the relative change is about 40%. Therefore, the contribution of the barotropic term in the 6-9–day waves is small compared to the 3-5–day waves. In the subtropical lower tropospheric generation center, C_k increases slightly due to dust-induced shortwave heating. In contrast to the 3-5–day case, the response near the tropopause associated with STJ is intense in the 6-9–day case.

Figure 8 depicts C_k over the Atlantic. In the 3-5–day waves, C_k associated with the shear of AEJ is intense but more confined to the jet core over the Atlantic compared to its continental counterpart. Unlike the continental case, dust causes an increase of C_k to the south of the AEJ core in all three cases, strengthening AEWs. The response is stronger than that over the continent. The response in the subtropical lower tropospheric positive C_k center is similar to its continental southern part but is more intense (75%). In the 6-9–day case also, C_k associated with the AEJ and its response to dust forcing is stronger over the Atlantic than the continent (Fig. 8 right column). As the dust shortwave absorption increases, more energy is converted to EKE. The energy generation in the 6-9–day AEWs associated with the C_k term is more sensitive to dust heating over the Atlantic than over continental Africa. The response in barotropic terms to the dust shortwave absorption is not as linear as in the baroclinic case, which might be because C_k involves four individual energy conversion terms, each of which interacts with dust forcing differently.

The next term in the energy cycle is the generation of EKE through diabatic heating,G_E (Fig. 9 and 10). The G_E has a very similar pattern to that of C_{pk} with two major generation centers at the subtropical lower and tropical upper troposphere. The similarity in the pattern of G_E and C_{pk} is because the G_E largely compensates for the A_E consumed by the C_{pk}. A positive G_E over the tropical upper troposphere is generated by the latent heat release from the precipitation, whereas the generation center over the subtropical lower troposphere (Sahara) is from dry convection and dust-induced diabatic heating. The magnitude of G_E is almost half that of C_{pk}.

The response of G_E to shortwave absorption is also very similar to that of C_{pk}, but its magnitude is smaller. However, the relative change in G_E is generally higher than that of C_{pk}. In the 3-5–day case, G_E enhances in both the tropical upper and subtropical lower tropospheric centers as the dust shortwave absorption increases. The former arises from the enhanced precipitation response to dust-radiative heating, and the latter is due to increased dust heating and possibly by the enhancement in the dry convection over this region. In the DUST2.7 case, approximately 50% increase occurs in the 3-5–day G_E compared to the NoDUST case.

In the 6-9–day case, the dipole response pattern in C_{pk} is replicated in G_E. The G_E is generated on the equator side and dissipated over the subtropics. The response intensifies as shortwave absorption increases. The response is consistent with the southward shift of 6-9–day AEWs as a response to dust shortwave heating. Approximately 75% change occurs in G_E on either side of the dipole. The subtropical lower tropospheric generation center also displays a strong response consistent with the C_{pk} response. That is, generation of G_E occurs in the less absorbing dust case, and destruction occurs in the high absorbing case.

Over the Atlantic, the generation of diabatic heating and its response to dust heating is smaller than the continental part (almost half). However, there is a significant decrease of G_E in the tropical lower troposphere under the upper tropospheric positive maxima region. The decrease in G_E at this location intensifies as the shortwave absorption increases.

Figures. 11 and 12 depicts the response in the conversion of zonal A_E to eddy A_E due to the eddy heat flux along the zonal mean temperature gradient, C_A. Unlike other terms, only one major location of zonal to eddy A_E conversion exists, starting from 12^0

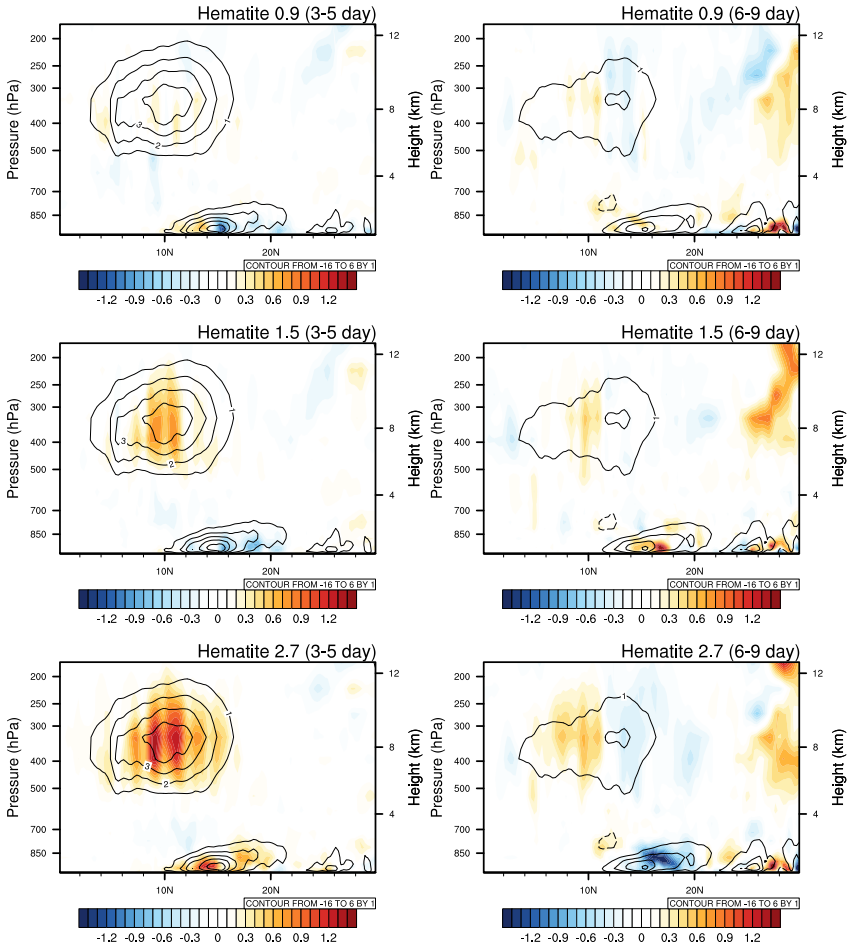

Figure 9. Meridional height cross-sections of the barotropic energy conversion term (G_E) averaged (15^0 W to 20^0 E) over the continental region. Contours represent the values of G_E in the "NoDUST" simulation, and the shaded contours represent anomalies (DUST-NoDUST) in all three dust experiments.

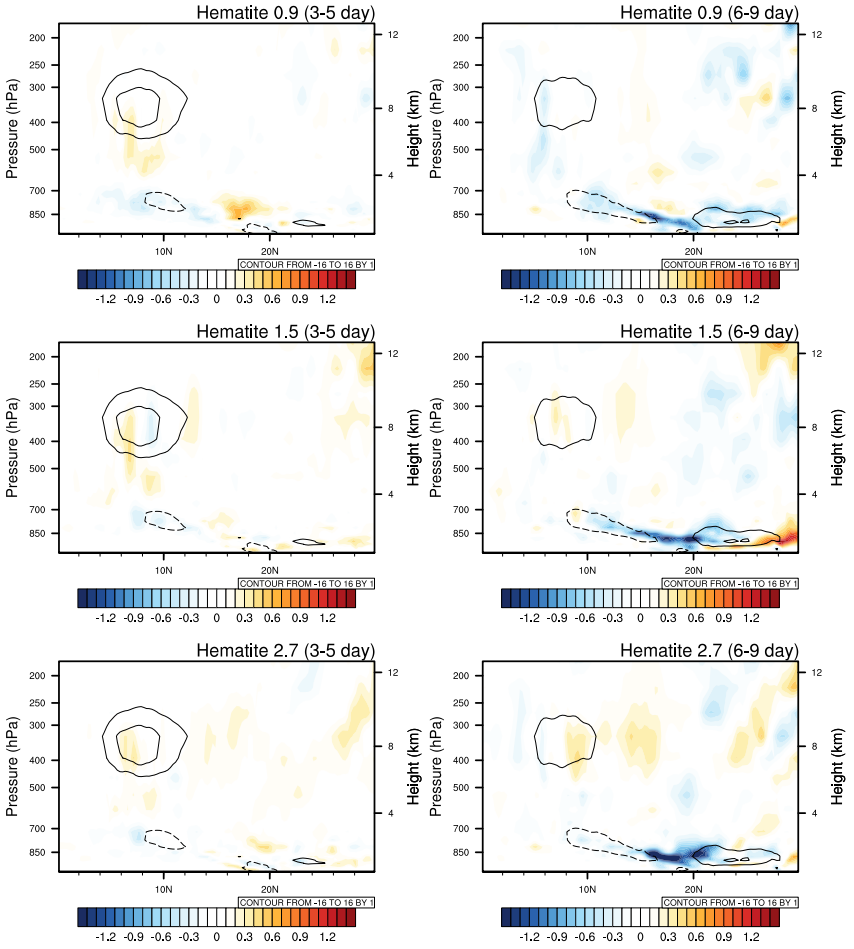

Figure 10. Same as Fig. 9, but averaged (50^0 W to 15^0 W) over the Atlantic.

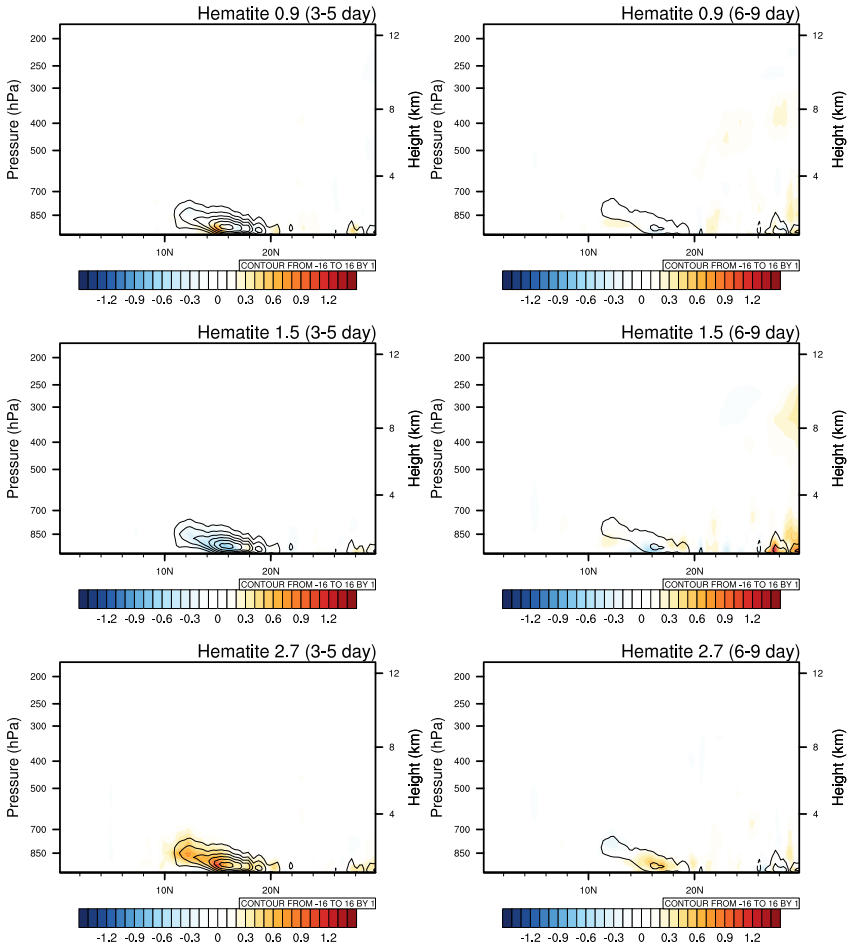

Figure 11. Meridional height cross-sections of the barotropic energy conversion term (C_A) averaged (15^0 W to 20^0 E) over the continental region. Contours represent the values of C_A in the "NoDUST" simulation, and the shaded contours represent anomalies (DUST-NoDUST) in all three dust experiments.

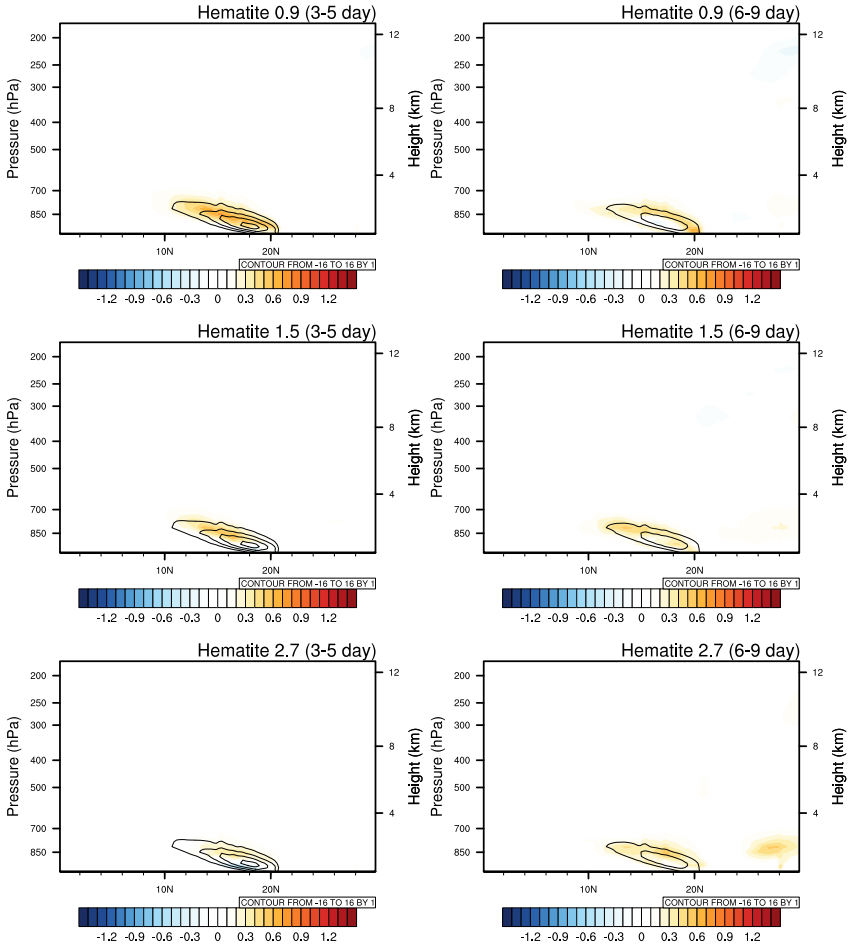

Figure 12. Same as Fig. 11, but averaged (50^0 W to 15^0 W) over the Atlantic.

N to 20^0 N in the lower troposphere (below 700 hPa). The magnitude of C_A over this region is comparable to G_E, indicating a comparable contribution to the baroclinic conversion over this region. The leading contribution in C_A results from the thermal advection by the large-scale meridional temperature gradient. The dust shortwave absorption heats the subtropical lower-mid troposphere, strengthening the meridional temperature gradient and C_A. In general, C_A increases with the dust shortwave absorption over the African continent (Fig. 11) and vice versa over the Atlantic (Fig. 12). The absolute magnitude of C_A and its response to dust heating is small for the 6-9–day case compared with the 3-5–day case.

4 Discussion and Summary

The radiative impact of mineral dust aerosols on AEWs over tropical Africa and the Atlantic has drawn scientific attention concerning their interactions since the 1970s. Although several studies have investigated the role of DDRF in AEW genesis and maintenance, less attention has been focused on the sensitivity of AEWs to the uncertainty in dust shortwave absorption. The present study conducted global high-resolution atmospheric simulations with the dust having various shortwave absorption properties to assess the sensitivity of the AEWs to dust-induced atmospheric heating rate. The anal-

yses were conducted separately for the 3-5–day and 6-9–day waves. We also analyzed the AEW's response over the African continent and the tropical Atlantic separately.

Generally, AEW activity intensifies and broadens the wave track in response to increased dust shortwave absorption and the consequent increase in atmospheric heating. The broadening of the track is primarily towards the equator, causing a southward shift of the track. The 6-9–day waves are more sensitive to dust shortwave absorption, compared to the 3-5–day wave, especially in terms of the percentage change. The 6-9–day waves weaken over the continent and the Atlantic in the inefficient absorbing case (DUST0.9), whereas they intensify and broaden over the Atlantic when the dust becomes an efficient absorber. The response over the continent is minimal, which is weakening of the 6-9–day waves in all three dust cases, leaving a stark land–sea contrast in the sensitivity of AEWs to dust heating. In the 3-5–day wave case, no evident land–sea contrast occurs in response to dust heating. When dust is an inefficient absorber, the 3-5–day waves weaken, except over the southern flank of the wave track. However, if dust efficiently absorbs shortwave radiation, the 3-5–day wave track intensifies and broadens in all directions.

We analyzed the response in various energetic terms to understand how dust-radiative heating interacts with AEW dynamics. Baroclinic energy conversion is the leading order term for the maintenance of AEWs. The next two vital terms are the barotropic energy conversion term and A_E generation via diabatic heating. Their magnitudes are almost half the magnitude of the Baroclinic conversion. For waves on the southern flank of the AEJ, which are mostly 3-5–day waves, the most crucial energy source is the baroclinic energy conversion associated with the tropical vertical overturning, followed by the zonal to eddy kinetic energy conversion associated with shear in AEJ. However, to the northern side of the AEJ core, where most of the 6-9–day waves occur, the source of energy perturbation is primarily from the baroclinic conversion associated with the subtropical dry convection and the northern edge of the tropical overturning. The contribution from the barotropic term is negligible or negative in the mid-troposphere to the north of the AEJ. However, intense production of barotropic energy conversion is confined to the layer of the atmosphere below 850 hPa. Note that the contribution of the generation of diabatic heating and conversion of zonal to eddy A_E reaches up to 700 hPa.

The sensitivity of AEWs to dust heating stems from a combination of the response from various energetic terms. Although baroclinic energy conversion is the leading order term, the response to dust shortwave heating in barotropic and generation terms is comparable to that in baroclinic conversion. In other words, the relative change (percentage change) is higher in barotropic and generation terms than in baroclinic terms in response to dust. As the dust shortwave absorption increases, baroclinic energy conversion increases in favor of the AEWs. However, baroclinic energy conversion reduces in response to dust heating and opposes AEW growth on the poleward side of the AEJ in 6-9–day waves over the continent. The response of barotropic energy conversion is not unidirectional. Over the land, barotropic energy conversion associated with the shear on the AEJ reduces and opposes AEW growth in low-absorbing dust cases and increases in favor of 3-5–day AEW growth in high-absorbing dust cases. However, the C_k associated with the shear in the trade wind over the Sahara increases in response to dust shortwave heating rate. In the 6-9–day case over land, significant reduction occurs in C_k around the jet core in both low and high-absorbing dust cases. Over the ocean, the C_k related to the shear on the AEJ and intertropical depression increases in all dust cases proportionally, in both 3-5–day and 6-9–day waves. The response in the generation term mimics the response in the baroclinic term. In addition, G_E increases in favor of AEWs in all cases, except for 6-9–day AEWs over the continent. In the 6-9–day case, G_E also produces a dipole pattern of response with the destruction of energy to the north and generation to the south in response to dust heating. Additionally, there is an intense reduction in the G_E in the lower troposphere centered around 20^0N over the Atlantic, in a 6-9–day case. Moreover, C_A increases in the subtropical lower troposphere below the jet

core as a response to dust heating. However, unlike other energetic terms, the C_A increase is maximum in the DUST0.9 case for 3-5–day waves over the Atlantic.

The land–sea contrast in the response of 6-9–day waves (weakening of EKE over the land and strengthening over the ocean) was mostly caused by the dipole pattern of response in C_{pk} and G_E, which could be understood as a response to enhanced precipitation and weakening of the overturning circulation. The enhanced precipitation and associated increase in the latent heat release ($T\prime$) dominate the response in C_{pk} in the tropics (south of the AEJ), and the reduced overturning circulation ($\omega\prime$) dominates the response north of AEJ.

In summary, AEWs are highly sensitive to dust shortwave absorption and consequent atmosphere heating. The EKE, the proxy for AEW activities, increases (decreases) by about 25% compared to NoDUST simulations over the AEW track when the dust is assumed to be an efficient absorber (inefficient absorber). It is noteworthy that the AEWs exhibit strong seasonal and interannual variabilities, which are expected to change with global warming. Moreover, the dust loading and their optical characteristics are also changing. Therefore, accurately representing dust optical properties is crucial for better predicting AEWs and the overall African climate.

Appendix A Energy Cycle Terms

The energy conversion terms are calculated as follows:

$$C_k = -\overline{\overrightarrow{V_H'}.(\overrightarrow{V'}.\nabla)\overrightarrow{V_H}} \tag{A1}$$

$$C_{pk} = -\frac{R}{p}\overline{\omega' T'} \tag{A2}$$

$$C_A = -\frac{c_p\gamma}{\overline{T}}\overline{\overrightarrow{V_H'}T'}.\nabla_H\overline{T} \tag{A3}$$

$$G_E = \frac{\gamma}{\overline{T}}\overline{Q_1' T'} \tag{A4}$$

where u and v are zonal and meridional velocities, ω represents the vertical pressure velocity, p denotes the pressure, and T denotes the temperature. In addition, $\gamma = \frac{\Gamma_d}{\Gamma_d - \Gamma}$, where Γ_d and Γ are the dry adiabatic and observed lapse rates, respectively. The c_p denotes the heat capacity at constant pressure, and R represents the dry air gas constant. Finally, σ is the dry static stability. Q_1 is the apparent heat source. The Q_1 is calculated as follows:

$$Q_1 = \frac{c_p T}{\theta}\left(\frac{\partial\theta}{\partial t} + u\frac{\partial\theta}{\partial\phi} + v\frac{\partial\theta}{\partial\lambda} + \omega\frac{\partial\theta}{\partial p}\right) \tag{A5}$$

where θ is the potential temperature.

Primes in these equations are calculated using the 3-5–day and 6-9–day Butterworth bandpass filter. The higher-order terms in (A1) and (A2) are omitted from the analysis. The positive and negative values in these figures represent the gain and loss of the EKE or eddy available potential energy, respectively.

Open Research

The source code of HiRAM is publicly available online (at https://www.gfdl.noaa.gov/hiram-quickstart/). The simulation results, figures, and code are available from the authors upon request.

Acknowledgments

The research reported in this publication was supported by funding from the King Abdullah University of Science and Technology (KAUST) through the Grant (BAS/1/1309-01-01) and Belmont Forum Grant (REP/1/3963-01-01/RFBR #20-55-75002), "Coastal OceAn SusTainability in Changing Climate (COAST)." For computer time, this research used the resources of the Supercomputing Laboratory at KAUST.

References

Balkanski, Y., Schulz, M., Claquin, T., & Guibert, S. (2007). Reevaluation of mineral aerosol radiative forcings suggests a better agreement with satellite and aeronet data. *Atmospheric Chemistry and Physics*, *7*(1), 81–95.

Bangalath, H. K., & Stenchikov, G. (2015). Role of dust direct radiative effect on the tropical rainbelt over middle east and north africa: A high resolution agcm study. *Journal of Geophysical Research: Atmospheres*, *120*, 4564–4584. doi: 10.1002/2015JD023122

Bangalath, H. K., & Stenchikov, G. (2016). Sensitivity of the middle east–north african tropical rainbelt to dust shortwave absorption: A high-resolution agcm experiment. *Journal of Climate*, *29*(19), 7103–7126.

Bercos-Hickey, E., Nathan, T. R., & Chen, S.-H. (2017). Saharan dust and the african easterly jet–african easterly wave system: Structure, location and energetics. *Quarterly Journal of the Royal Meteorological Society*, *143*(708), 2797-2808. Retrieved from `https://rmets.onlinelibrary.wiley.com/doi/abs/10.1002/qj.3128` doi: https://doi.org/10.1002/qj.3128

Bercos-Hickey, E., Nathan, T. R., & Chen, S.-H. (2022). Effects of saharan dust aerosols and west african precipitation on the energetics of african easterly waves. *Journal of the Atmospheric Sciences*, *79*(7), 1911–1926.

Boyle, J., & Klein, S. A. (2010). Impact of horizontal resolution on climate model forecasts of tropical precipitation and diabatic heating for the twp-ice period. *Journal of Geophysical Research: Atmospheres*, *115*(D23).

Carlson, T. N., & Prospero, J. M. (1972). The large-scale movement of saharan air outbreaks over the northern equatorial atlantic. *Journal of Applied Meteorology and Climatology*, *11*(2), 283–297.

Cornforth, R. J., Hoskins, B. J., & Thorncroft, C. D. (2009). The impact of moist processes on the african easterly jet–african easterly wave system. *Quarterly Journal of the Royal Meteorological Society: A journal of the atmospheric sciences, applied meteorology and physical oceanography*, *135*(641), 894–913.

Diedhiou, A., Janicot, S., Viltard, A., & De Félice, P. (2002). Energetics of easterly wave disturbances over west africa and the tropical atlantic: A climatology from the 1979–95 ncep/ncar reanalyses. *Climate dynamics*, *18*, 487–500.

Grogan, D. F., Nathan, T. R., & Chen, S.-H. (2016). Effects of saharan dust on the linear dynamics of african easterly waves. *Journal of the Atmospheric Sciences*, *73*(2), 891–911.

Grogan, D. F., Nathan, T. R., & Chen, S.-H. (2017). Saharan dust and the nonlinear evolution of the african easterly jet–african easterly wave system. *Journal of the Atmospheric Sciences*, *74*(1), 27–47.

Grogan, D. F., & Thorncroft, C. D. (2019). The characteristics of african easterly waves coupled to saharan mineral dust aerosols. *Quarterly Journal of the Royal Meteorological Society*, *145*(720), 1130–1146.

Hall, N. M., Kiladis, G. N., & Thorncroft, C. D. (2006). Three-dimensional structure and dynamics of african easterly waves. part ii: Dynamical modes. *Journal of the atmospheric sciences*, *63*(9), 2231–2245.

Haywood, J., Francis, P., Osborne, S., Glew, M., Loeb, N., Highwood, E., ... Hirst, E. (2003). Radiative properties and direct radiative effect of saharan dust measured by the c-130 aircraft during shade: 1. solar spectrum. *Journal of*

Geophysical Research: Atmospheres, *108*(D18). Retrieved from https://agupubs.onlinelibrary.wiley.com/doi/abs/10.1029/2002JD002687 doi: https://doi.org/10.1029/2002JD002687

Haywood, J. M., Francis, P. N., Glew, M. D., & Taylor, J. P. (2001). Optical properties and direct radiative effect of saharan dust: A case study of two saharan dust outbreaks using aircraft data. *Journal of Geophysical Research: Atmospheres*, *106*(D16), 18417-18430. Retrieved from https://agupubs.onlinelibrary.wiley.com/doi/abs/10.1029/2000JD900319 doi: https://doi.org/10.1029/2000JD900319

Hsieh, J.-S., & Cook, K. H. (2007). A study of the energetics of african easterly waves using a regional climate model. *Journal of the Atmospheric Sciences*, *64*(2), 421-440. Retrieved from https://doi.org/10.1175/JAS3851.1 doi: 10.1175/JAS3851.1

Jones, C., Mahowald, N., & Luo, C. (2004). Observational evidence of african desert dust intensification of easterly waves. *Geophysical research letters*, *31*(17).

Jung, T., Miller, M., Palmer, T., Towers, P., Wedi, N., Achuthavarier, D., ... others (2012). High-resolution global climate simulations with the ecmwf model in project athena: Experimental design, model climate, and seasonal forecast skill. *Journal of Climate*, *25*(9), 3155–3172.

Jury, M. R., & Santiago, M. J. (2010). Composite analysis of dust impacts on african easterly waves in the moderate resolution imaging spectrometer era. *Journal of Geophysical Research: Atmospheres*, *115*(D16).

Karyampudi, V. M., & Carlson, T. N. (1988). Analysis and numerical simulations of the saharan air layer and its effect on easterly wave disturbances. *Journal of the Atmospheric Sciences*, *45*(21), 3102–3136.

Kaufman, Y. J., Tanré, D., Dubovik, O., Karnieli, A., & Remer, L. A. (2001). Absorption of sunlight by dust as inferred from satellite and ground-based remote sensing. *Geophysical Research Letters*, *28*(8), 1479-1482. Retrieved from https://agupubs.onlinelibrary.wiley.com/doi/abs/10.1029/2000GL012647 doi: https://doi.org/10.1029/2000GL012647

Landsea, C. W. (1993). A climatology of intense (or major) atlantic hurricanes. *Monthly Weather Review*, *121*(6), 1703 - 1713. Retrieved from https://journals.ametsoc.org/view/journals/mwre/121/6/1520-0493_1993_121_1703_acoima_2_0_co_2.xml doi: 10.1175/1520-0493(1993)121⟨1703:ACOIMA⟩2.0.CO;2

Lau, N.-C., & Ploshay, J. J. (2009). Simulation of synoptic-and subsynoptic-scale phenomena associated with the east asian summer monsoon using a high-resolution gcm. *Monthly Weather Review*, *137*(1), 137–160.

Lavaysse, C., Chaboureau, J.-P., & Flamant, C. (2011). Dust impact on the west african heat low in summertime. *Quarterly Journal of the Royal Meteorological Society*, *137*(658), 1227-1240. Retrieved from https://rmets.onlinelibrary.wiley.com/doi/abs/10.1002/qj.844 doi: https://doi.org/10.1002/qj.844

Lorenz, E. N. (1955). Available potential energy and the maintenance of the general circulation. *Tellus*, *7*(2), 157–167.

Ma, P.-L., Zhang, K., Shi, J. J., Matsui, T., & Arking, A. (2012). Direct radiative effect of mineral dust on the development of african easterly waves in late summer, 2003–07. *Journal of applied meteorology and climatology*, *51*(12), 2090–2104.

Miller, R., Perlwitz, J., & Tegen, I. (2004). Feedback upon dust emission by dust radiative forcing through the planetary boundary layer. *Journal of Geophysical Research: Atmospheres*, *109*(D24).

Muench, H. S. (1965). On the dynamics of the wintertime stratosphere circulation. *Journal of Atmospheric Sciences*, *22*(4), 349 - 360. Retrieved from https://journals.ametsoc.org/view/journals/atsc/22/4/1520-0469_1965_022_0349_otdotw_2_0_co_2.xml doi: 10.1175/1520-0469(1965)022⟨0349:

OTDOTW⟩2.0.CO;2

Nathan, T. R., Grogan, D. F., & Chen, S.-H. (2017). Subcritical destabilization of african easterly waves by saharan mineral dust. *Journal of the Atmospheric Sciences*, *74*(4), 1039–1055.

Norquist, D. C., Recker, E. E., & Reed, R. J. (1977). The energetics of african wave disturbances as observed during phase iii of gate. *Monthly Weather Review*, *105*(3), 334–342.

Osipov, S., Stenchikov, G., Brindley, H., & Banks, J. (2015). Diurnal cycle of the dust instantaneous direct radiative forcing over the arabian peninsula. *Atmospheric Chemistry and Physics*, *15*(16), 9537–9553.

Otto, S., Bierwirth, E., Weinzierl, B., Kandler, K., Esselborn, M., Tesche, M., ... Trautmann, T. (2009). Solar radiative effects of a saharan dust plume observed during samum assuming spheroidal model particles. *Tellus B: Chemical and Physical Meteorology*, *61*(1), 270–296.

Patricola, C. M., Saravanan, R., & Chang, P. (2018). The response of atlantic tropical cyclones to suppression of african easterly waves. *Geophysical Research Letters*, *45*(1), 471-479. Retrieved from `https://agupubs.onlinelibrary.wiley.com/doi/abs/10.1002/2017GL076081` doi: https://doi.org/10.1002/2017GL076081

Raj, J., Bangalath, H. K., & Stenchikov, G. L. (2022). Future projection of the african easterly waves in a high-resolution atmospheric general circulation model.
doi: https://doi.org/10.21203/rs.3.rs-1501278/v1

Raut, J.-C., & Chazette, P. (2008). Radiative budget in the presence of multilayered aerosol structures in the framework of amma sop-0. *Atmospheric Chemistry and Physics*, *8*(22), 6839–6864.

Rayner, N., Parker, D. E., Horton, E., Folland, C. K., Alexander, L. V., Rowell, D., ... Kaplan, A. (2003). Global analyses of sea surface temperature, sea ice, and night marine air temperature since the late nineteenth century. *Journal of Geophysical Research: Atmospheres*, *108*(D14).

Reale, O., Lau, W. K., Kim, K.-M., & Brin, E. (2009). Atlantic tropical cyclogenetic processes during sop-3 namma in the geos-5 global data assimilation and forecast system. *Journal of the atmospheric sciences*, *66*(12), 3563–3578.

Russell, J. O., Aiyyer, A., White, J. D., & Hannah, W. (2017). Revisiting the connection between african easterly waves and atlantic tropical cyclogenesis. *Geophysical Research Letters*, *44*(1), 587-595. Retrieved from `https://agupubs.onlinelibrary.wiley.com/doi/abs/10.1002/2016GL071236` doi: https://doi.org/10.1002/2016GL071236

Slingo, A., Ackerman, T. P., Allan, R. P., Kassianov, E. I., McFarlane, S. A., Robinson, G. J., ... Dewitte, S. (2006). Observations of the impact of a major saharan dust storm on the atmospheric radiation balance. *Geophysical Research Letters*, *33*(24). Retrieved from `https://agupubs.onlinelibrary.wiley.com/doi/abs/10.1029/2006GL027869` doi: https://doi.org/10.1029/2006GL027869

Solmon, F., Mallet, M., Elguindi, N., Giorgi, F., Zakey, A., & Konaré, A. (2008). Dust aerosol impact on regional precipitation over western africa, mechanisms and sensitivity to absorption properties. *Geophysical Research Letters*, *35*(24).

Thorncroft, C. D., & Hoskins, B. J. (1994a). An idealized study of african easterly waves. i: A linear view. *Quarterly Journal of the Royal Meteorological Society*, *120*(518), 953-982. Retrieved from `https://rmets.onlinelibrary.wiley.com/doi/abs/10.1002/qj.49712051809` doi: https://doi.org/10.1002/qj.49712051809

Thorncroft, C. D., & Hoskins, B. J. (1994b). An idealized study of african easterly waves. i: A linear view. *Quarterly Journal of the Royal Meteorological Society*, *120*(518), 953-982. Retrieved from `https://rmets`

.onlinelibrary.wiley.com/doi/abs/10.1002/qj.49712051809 doi: https://doi.org/10.1002/qj.49712051809

Yanai, M. (1961). Dynamical aspects of typhoon formation. *Journal of the Meteorological Society of Japan. Ser. II*, *39*(5), 282–309.

Zhao, M., Held, I. M., Lin, S.-J., & Vecchi, G. A. (2009). Simulations of global hurricane climatology, interannual variability, and response to global warming using a 50-km resolution gcm. *Journal of Climate*, *22*(24), 6653–6678. doi: 10.1175/2009JCLI3049.1

Net_HeatingMeridionaMENA_land_JJA09.eps.

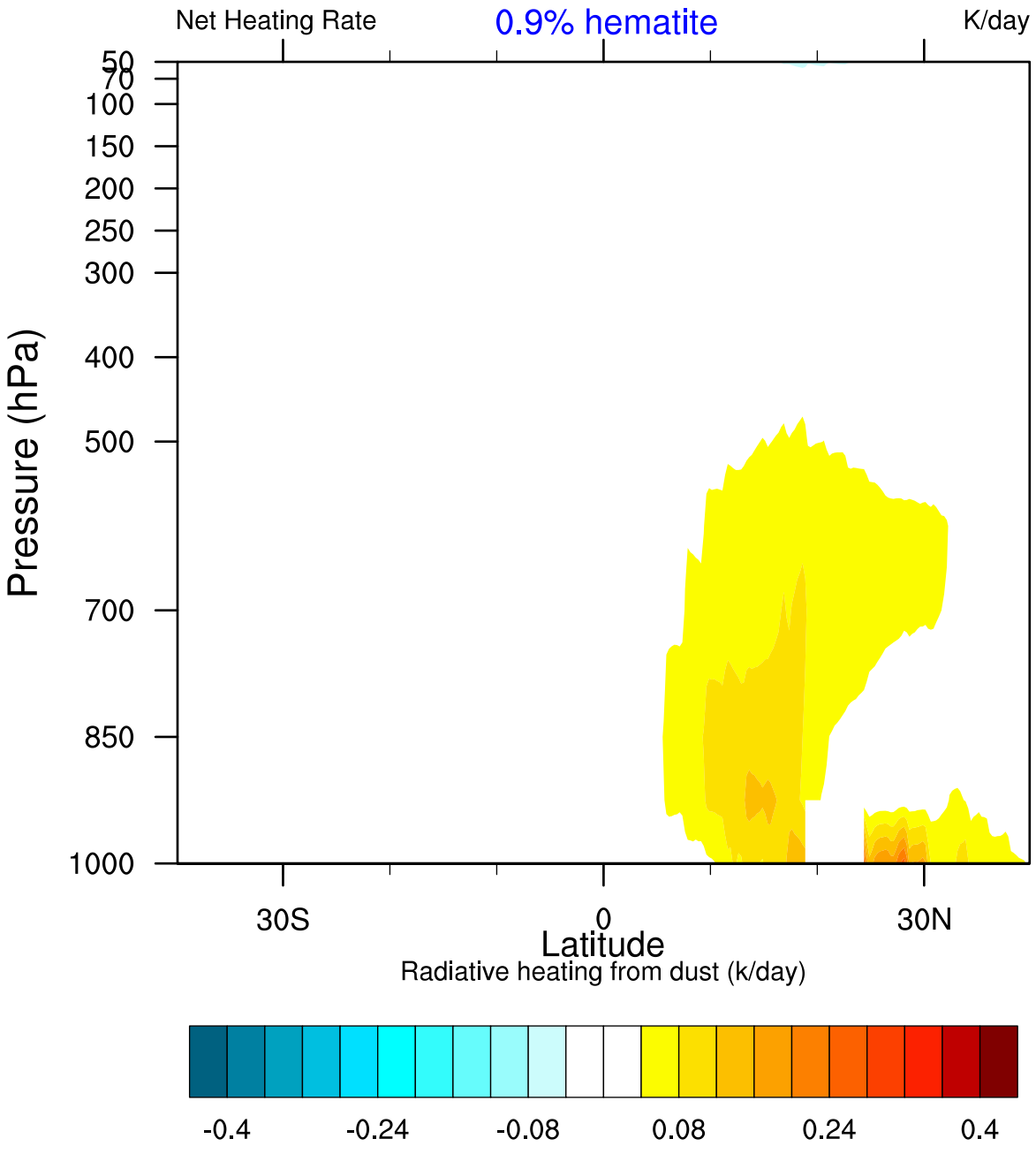
Net Heating Rate
0.9% hematite
K/day
50
70
100
150
200
250
300
400
500
700
850
1000
Pressure (hPa)
30S
0
30N
Latitude
Radiative heating from dust (k/day)
-0.4
-0.24
-0.08
0.08
0.24
0.4

Net_HeatingMeridionaMENA_ocean_JJA09.eps.

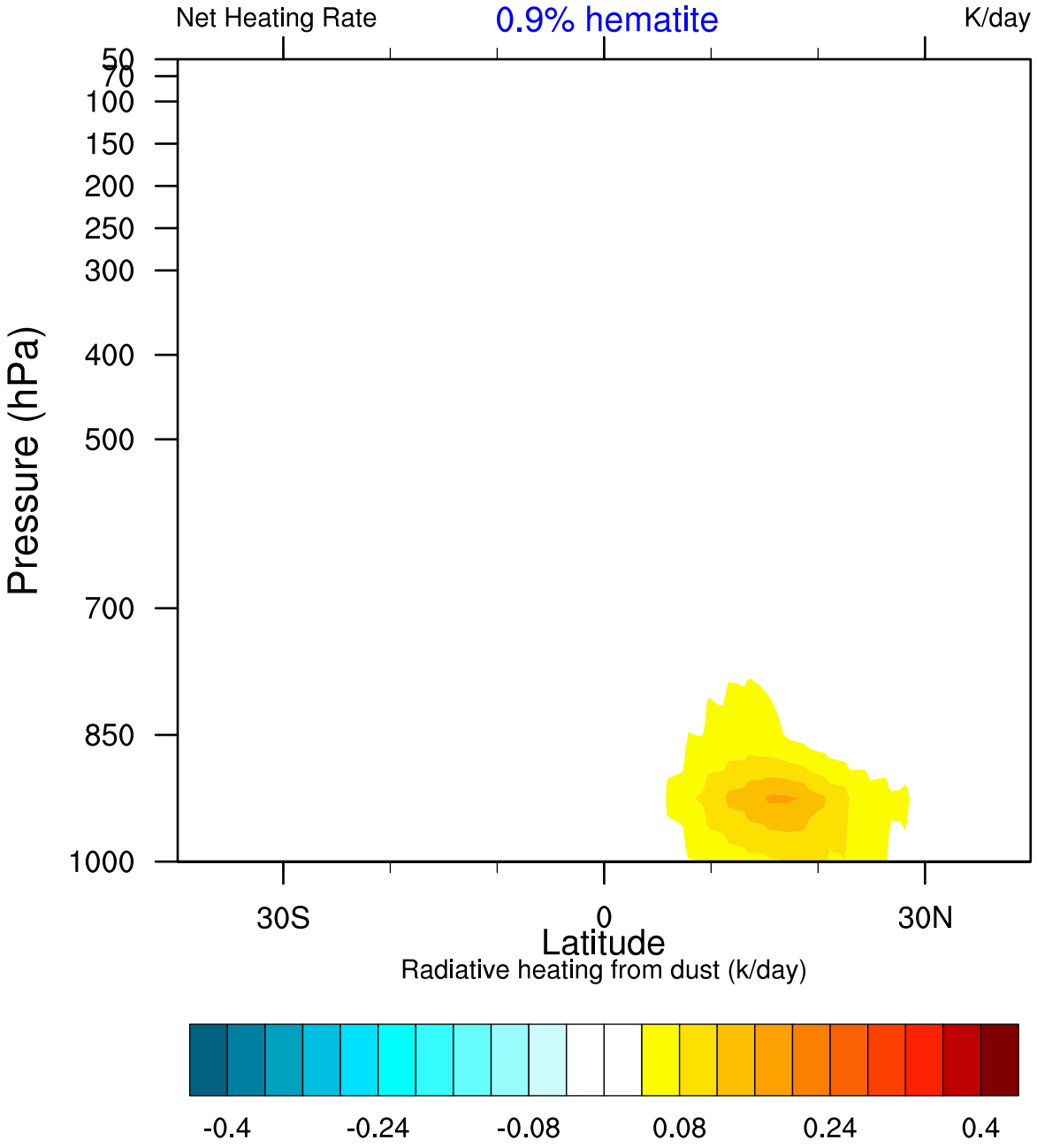
Net Heating Rate
0.9% hematite
K/day
50
70
100
150
200
250
300
400
500
700
850
1000
Pressure (hPa)
30S
0
30N
Latitude
Radiative heating from dust (k/day)
-0.4
-0.24
-0.08
0.08
0.24
0.4

Net_HeatingMeridionaMENA_land_JJA27.eps.

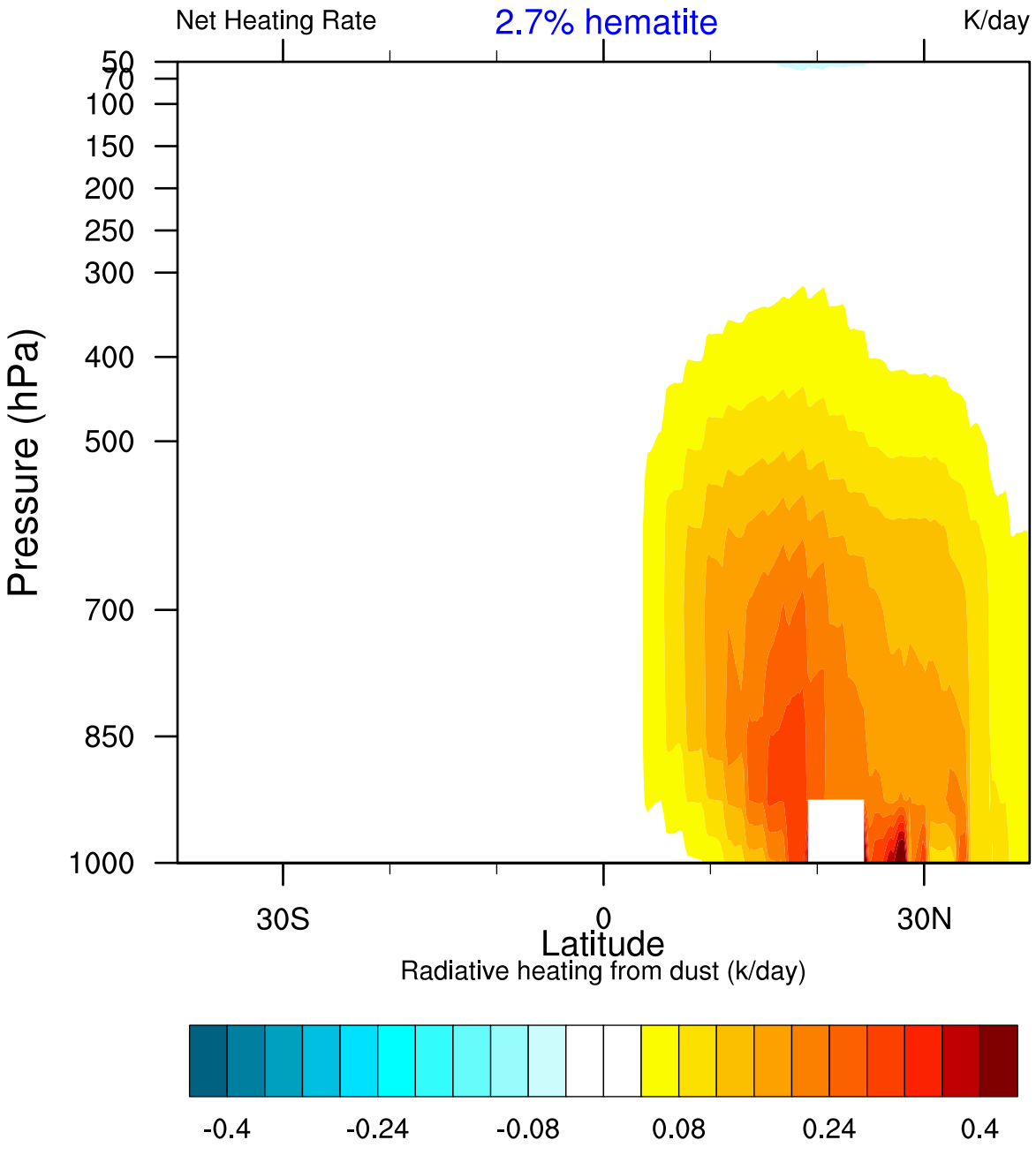
Net Heating Rate
2.7% hematite
K/day
50
70
100
150
200
250
300
400
500
700
850
1000
Pressure (hPa)
30S
0
30N
Latitude
Radiative heating from dust (k/day)
-0.4
-0.24
-0.08
0.08
0.24
0.4

Net_HeatingMeridionaMENA_land_JJA15.eps.

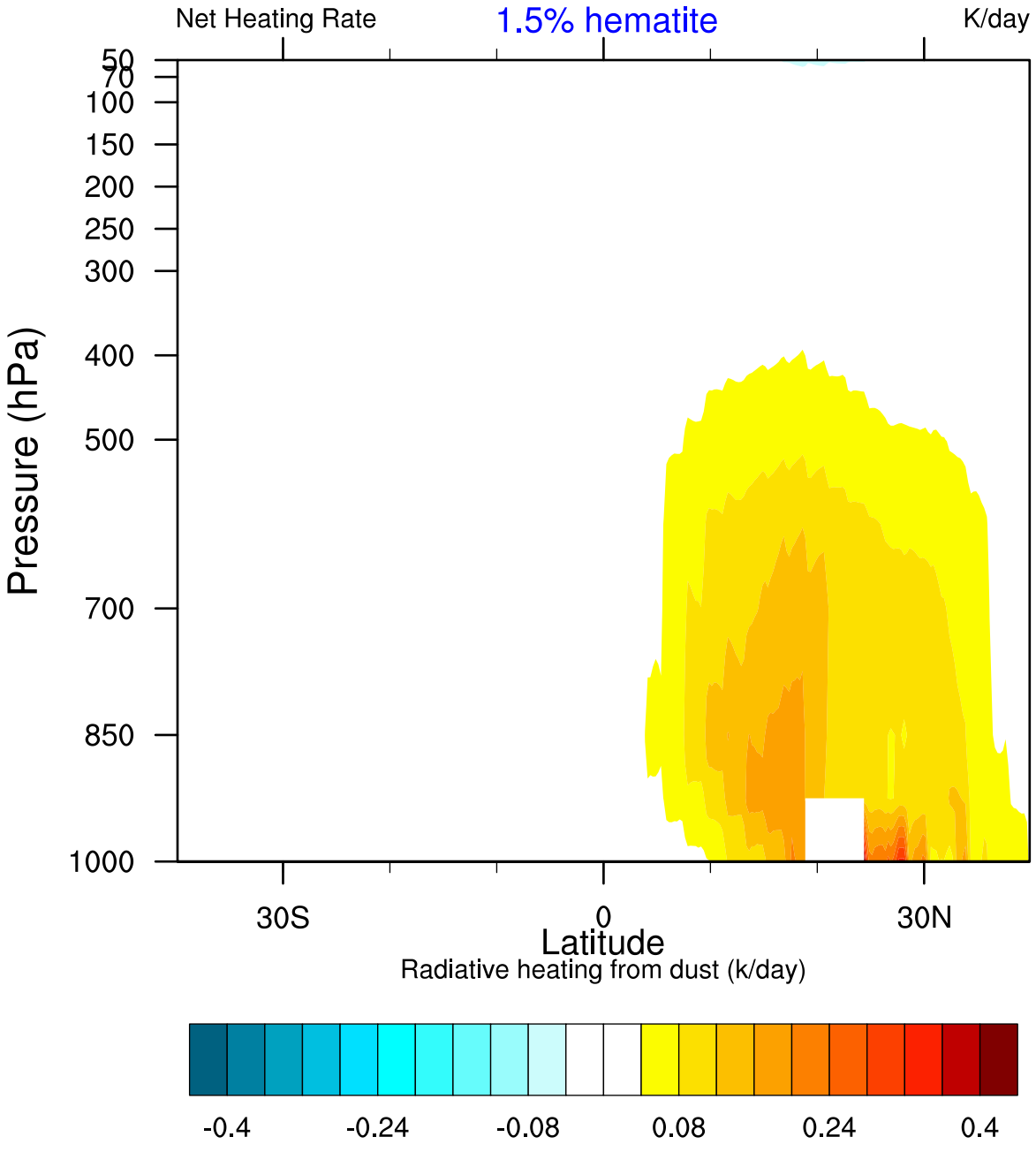
Net Heating Rate
1.5% hematite
K/day
50
70
100
150
200
250
300
400
500
700
850
1000
Pressure (hPa)
30S
0
30N
Latitude
Radiative heating from dust (k/day)
-0.4
-0.24
-0.08
0.08
0.24
0.4

DDRF_TOA_ALL_MENA_JJAS.eps.

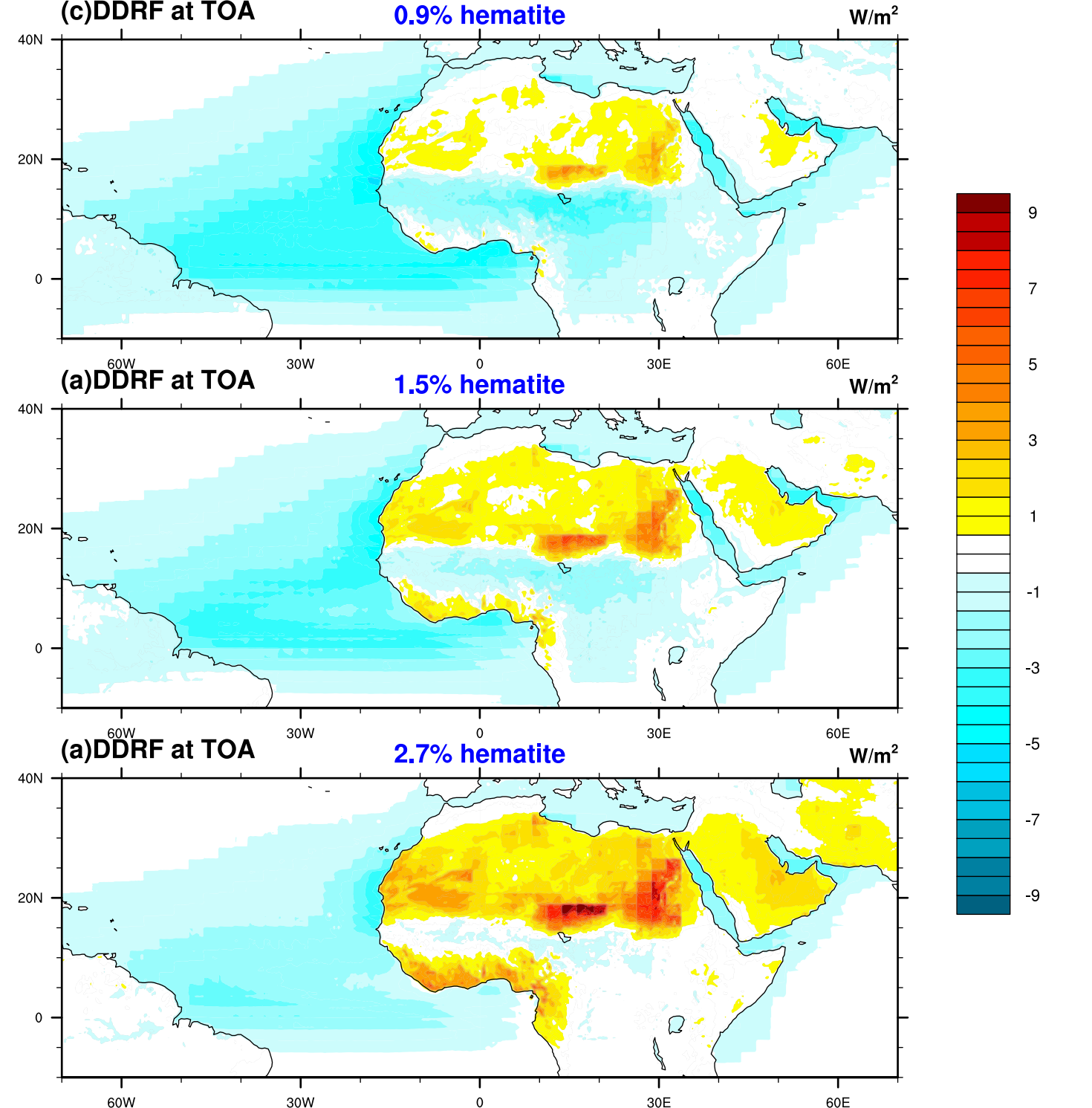
(c)DDRF at TOA
0.9% hematite
W/m²
40N
20N
0
60W
30W
0
30E
60E
(a)DDRF at TOA
1.5% hematite
W/m²
40N
20N
0
60W
30W
0
30E
60E
(a)DDRF at TOA
2.7% hematite
W/m²
40N
20N
0
60W
30W
0
30E
60E
9
7
5
3
1
-1
-3
-5
-7
-9

bc_ocean.eps.

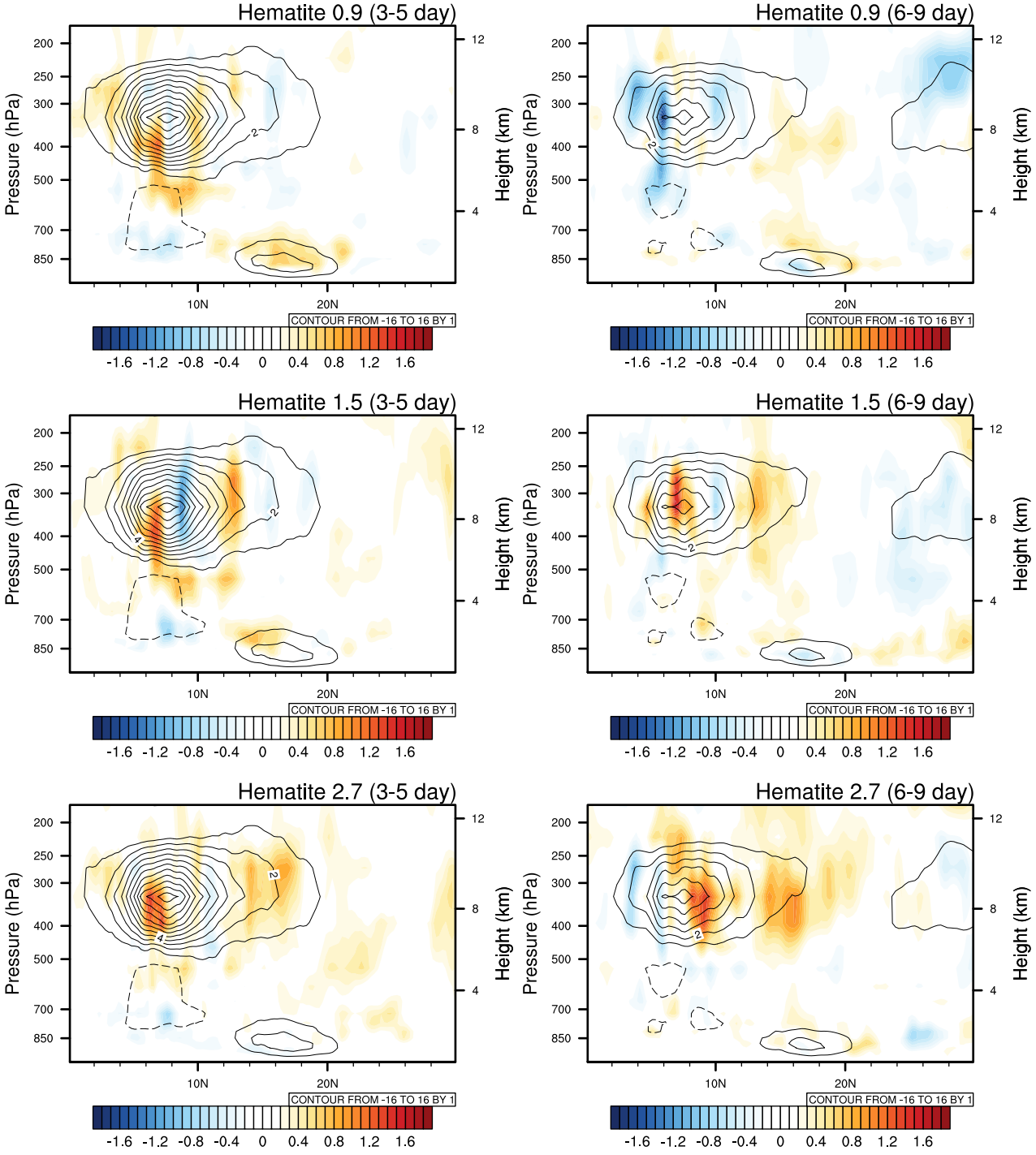
Hematite 0.9 (3-5 day)
Hematite 0.9 (6-9 day)
Hematite 1.5 (3-5 day)
Hematite 1.5 (6-9 day)
Hematite 2.7 (3-5 day)
Hematite 2.7 (6-9 day)
Pressure (hPa)
Height (km)
200
250
300
400
500
700
850
12
8
4
10N
20N
CONTOUR FROM -16 TO 16 BY 1
-1.6 -1.2 -0.8 -0.4 0 0.4 0.8 1.2 1.6

Net_HeatingMeridionaMENA_ocean_JJA27.eps.

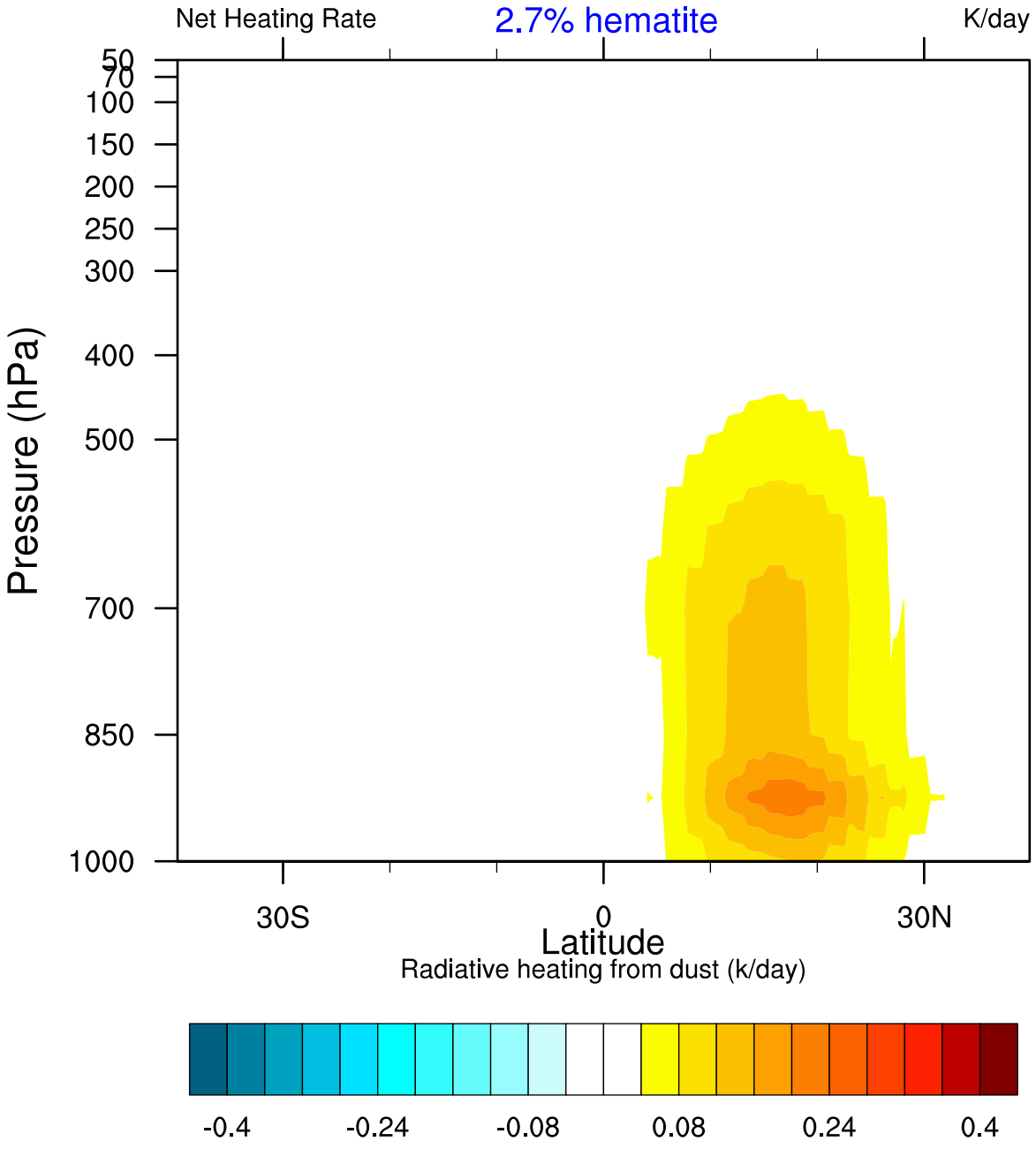
Net Heating Rate
2.7% hematite
K/day
50
70
100
150
200
250
300
400
500
700
850
1000
Pressure (hPa)
30S
0
30N
Latitude
Radiative heating from dust (k/day)
-0.4
-0.24
-0.08
0.08
0.24
0.4

bpf_35_olr_bias.eps.

Hematite0.9 - No Dust (3 - 5 days)

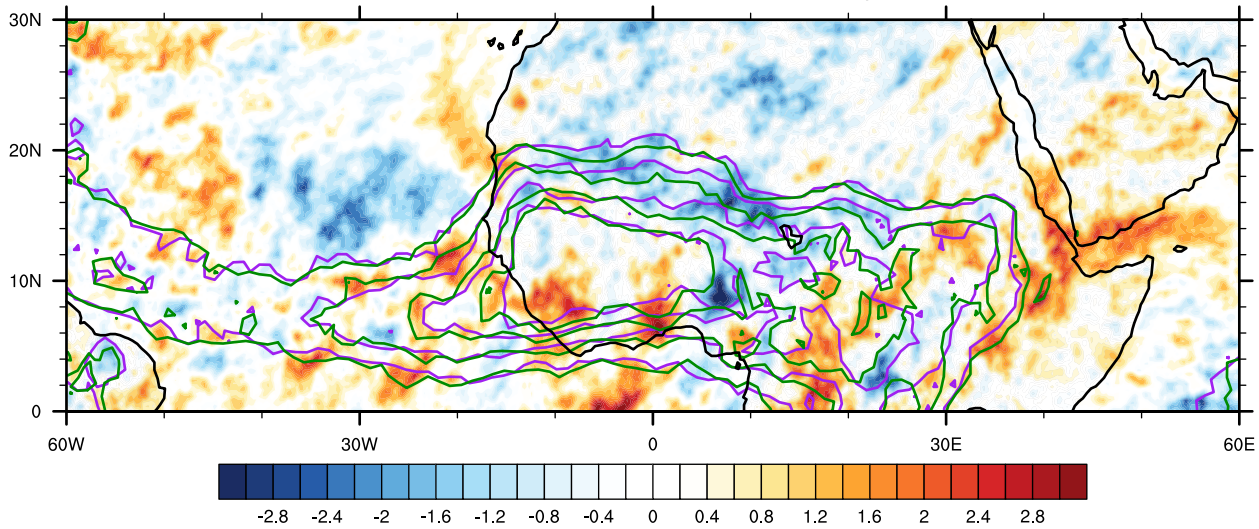

CONTOUR FROM 13 TO 21 BY 3

Hematite1.5 - No Dust (3 - 5 days)

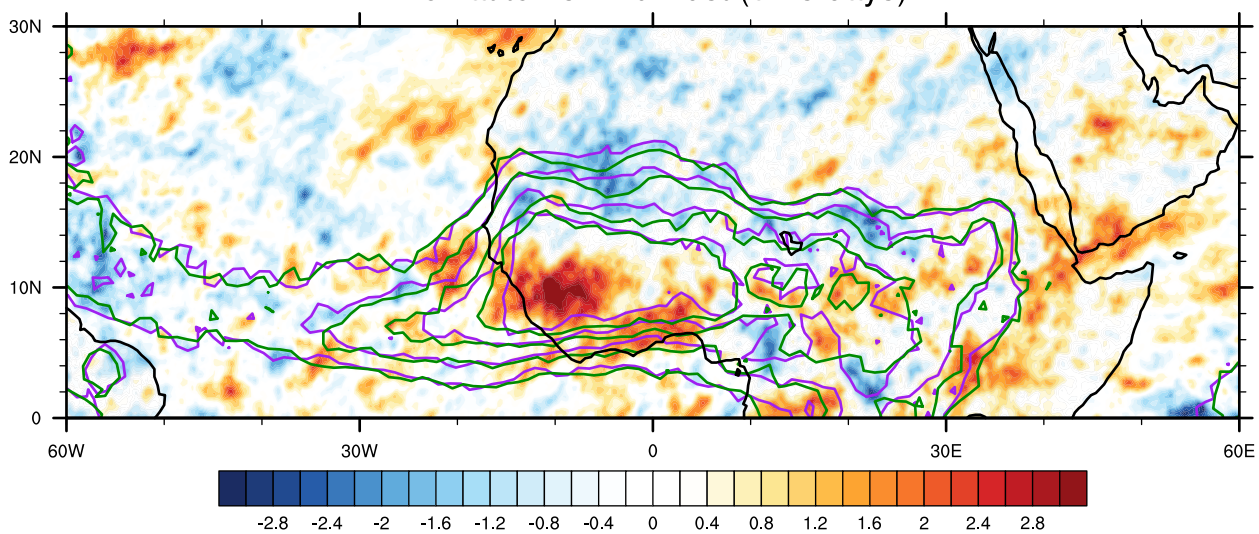

CONTOUR FROM 13 TO 21 BY 3

Hematite2.7 - No Dust (3 - 5 days)

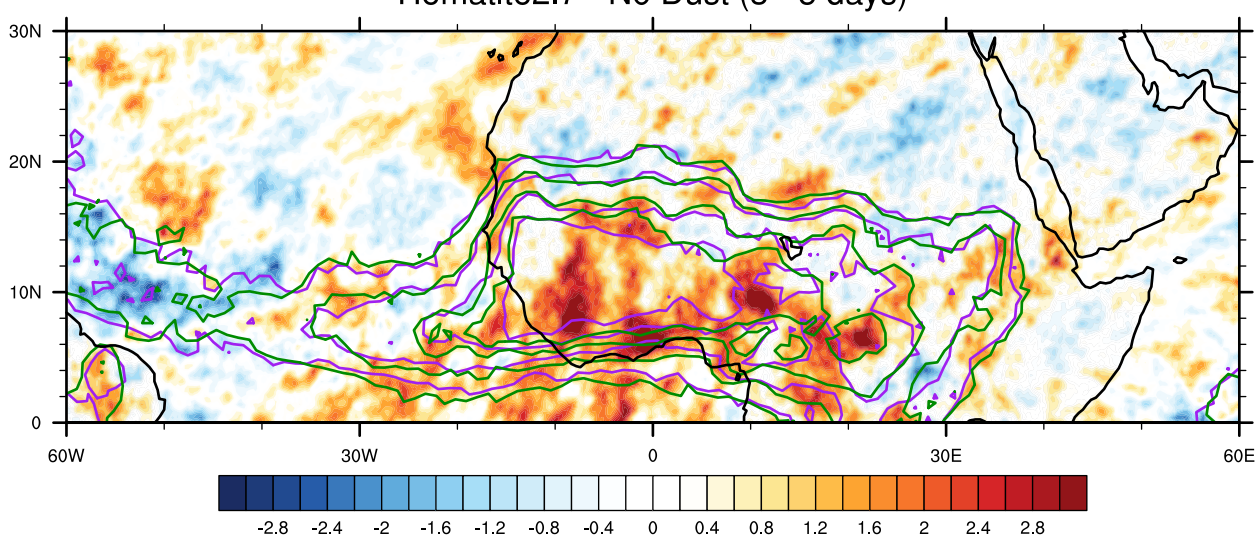

CONTOUR FROM 13 TO 21 BY 3

Net_HeatingMeridionaMENA_ocean_JJA15.eps.

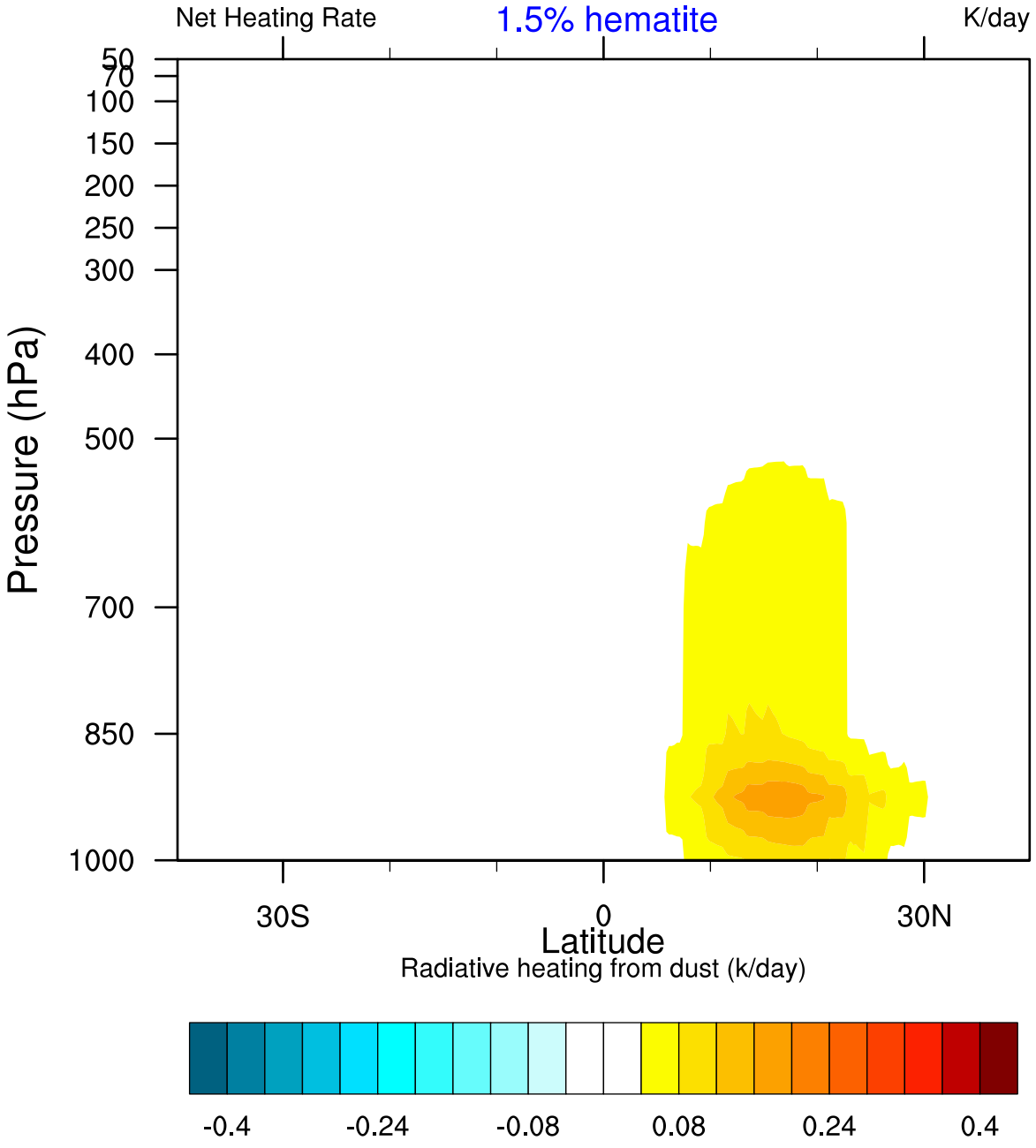
Net Heating Rate
1.5% hematite
K/day
50
70
100
150
200
250
300
400
500
700
850
1000
Pressure (hPa)
30S
0
30N
Latitude
Radiative heating from dust (k/day)
-0.4
-0.24
-0.08
0.08
0.24
0.4

bpf_35_bias.png.

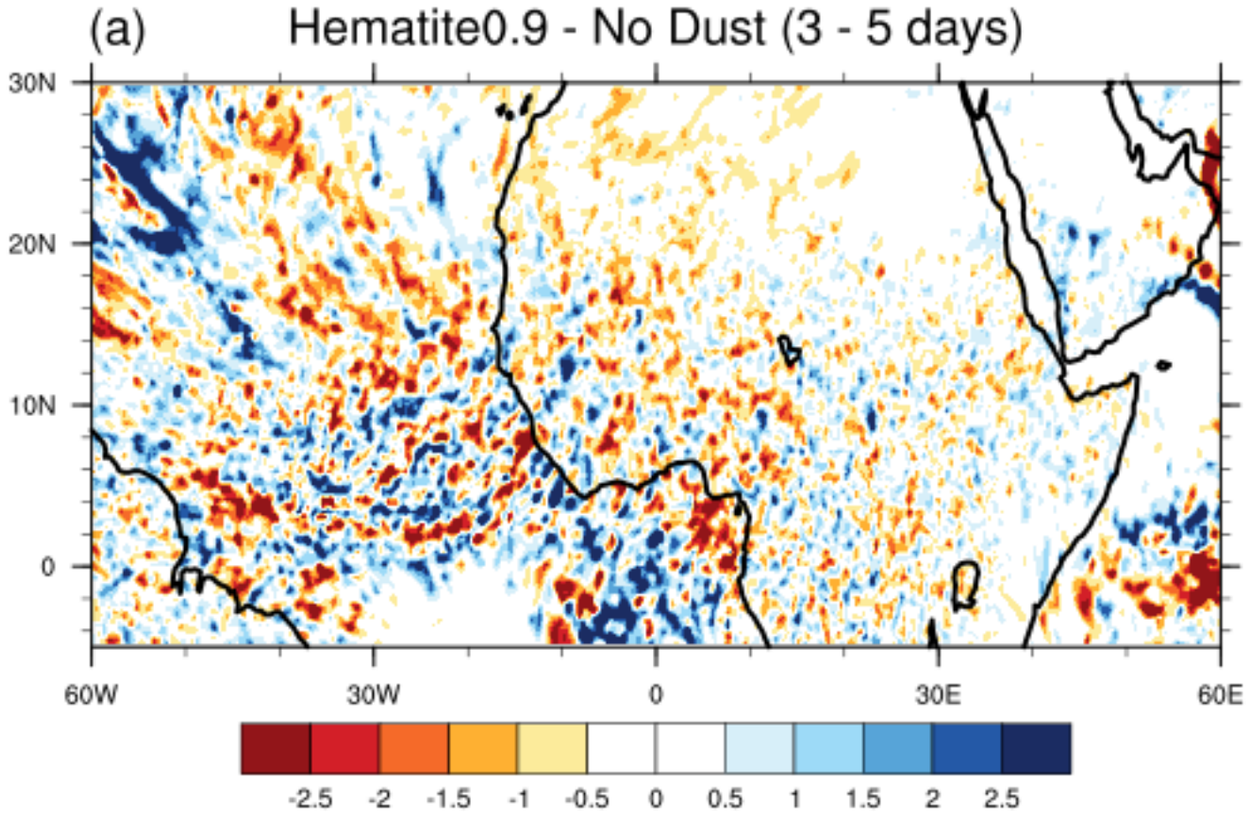
(a) Hematite0.9 - No Dust (3 - 5 days)
30N
20N
10N
0
60W
30W
0
30E
60E
-2.5 -2 -1.5 -1 -0.5 0 0.5 1 1.5 2 2.5

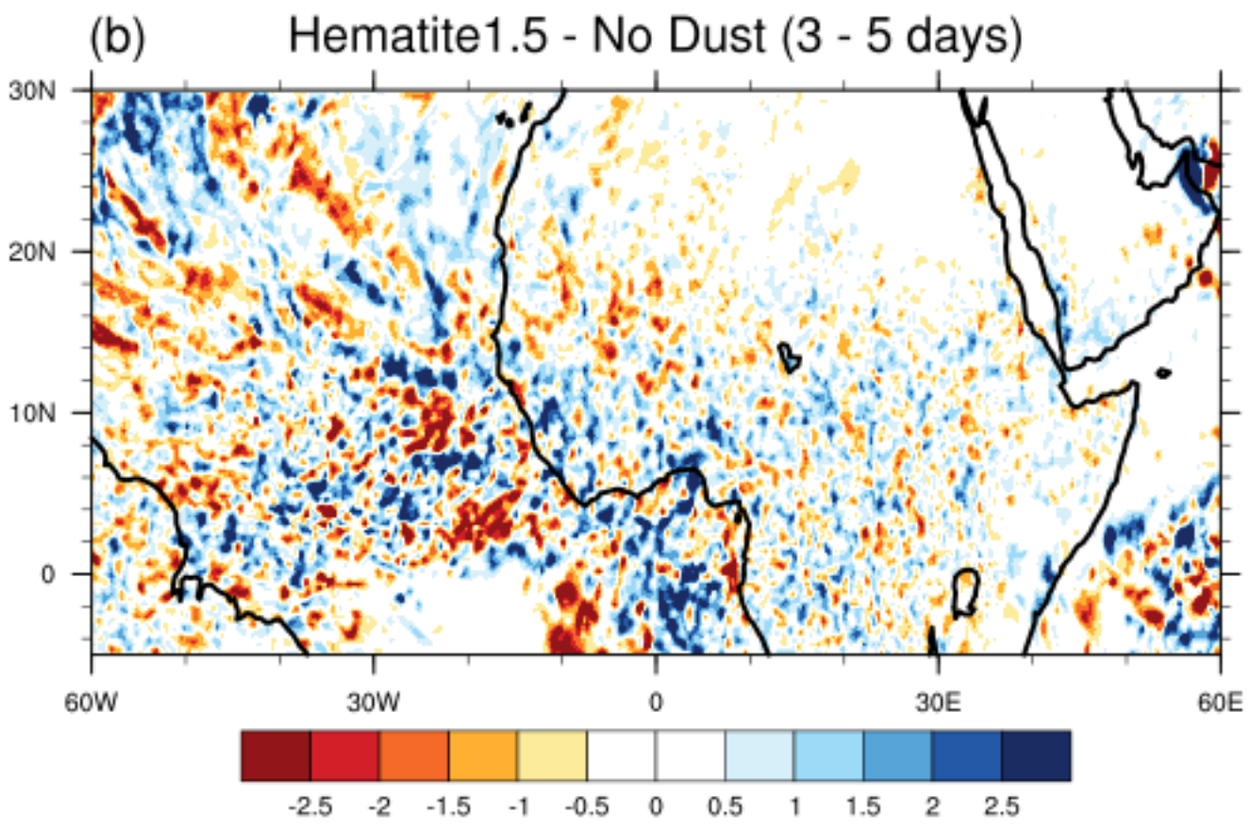
(b) Hematite1.5 - No Dust (3 - 5 days)
30N
20N
10N
0
60W
30W
0
30E
60E
-2.5 -2 -1.5 -1 -0.5 0 0.5 1 1.5 2 2.5

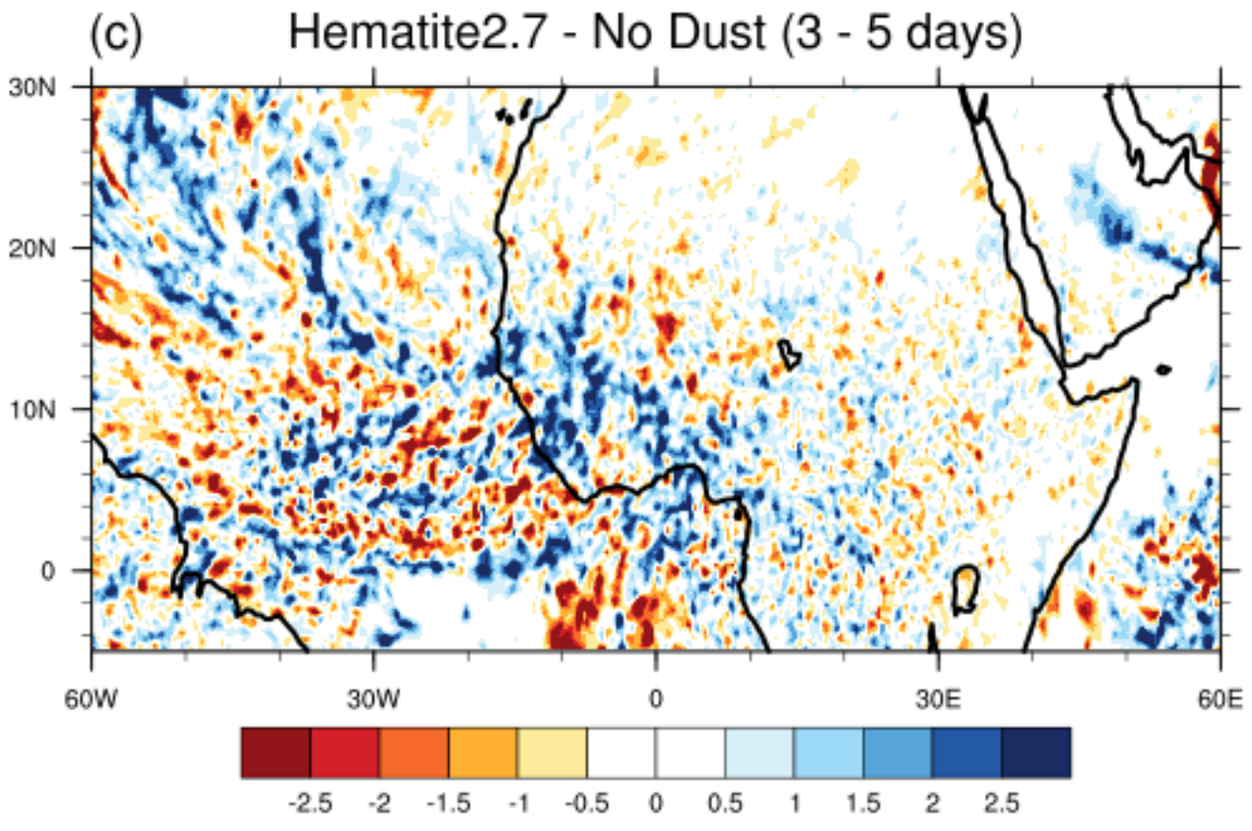
(c) Hematite2.7 - No Dust (3 - 5 days)
30N
20N
10N
0
60W
30W
0
30E
60E
-2.5 -2 -1.5 -1 -0.5 0 0.5 1 1.5 2 2.5

bc_land.eps.

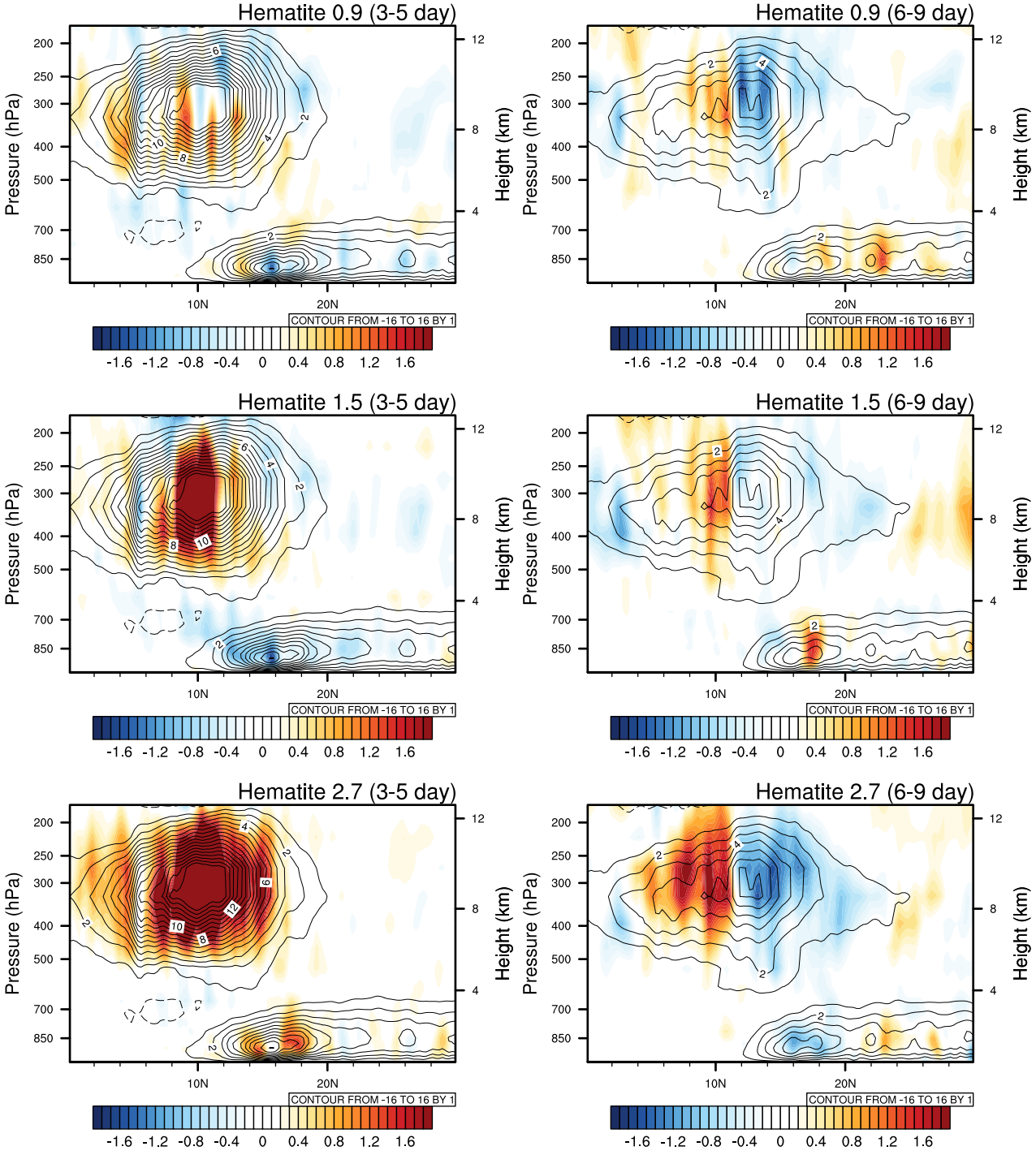
Hematite 0.9 (3-5 day)
Hematite 0.9 (6-9 day)
Hematite 1.5 (3-5 day)
Hematite 1.5 (6-9 day)
Hematite 2.7 (3-5 day)
Hematite 2.7 (6-9 day)
Pressure (hPa)
Height (km)
200
250
300
400
500
700
850
12
8
4
10N
20N
CONTOUR FROM -16 TO 16 BY 1
-1.6 -1.2 -0.8 -0.4 0 0.4 0.8 1.2 1.6

bt_ocean.eps.

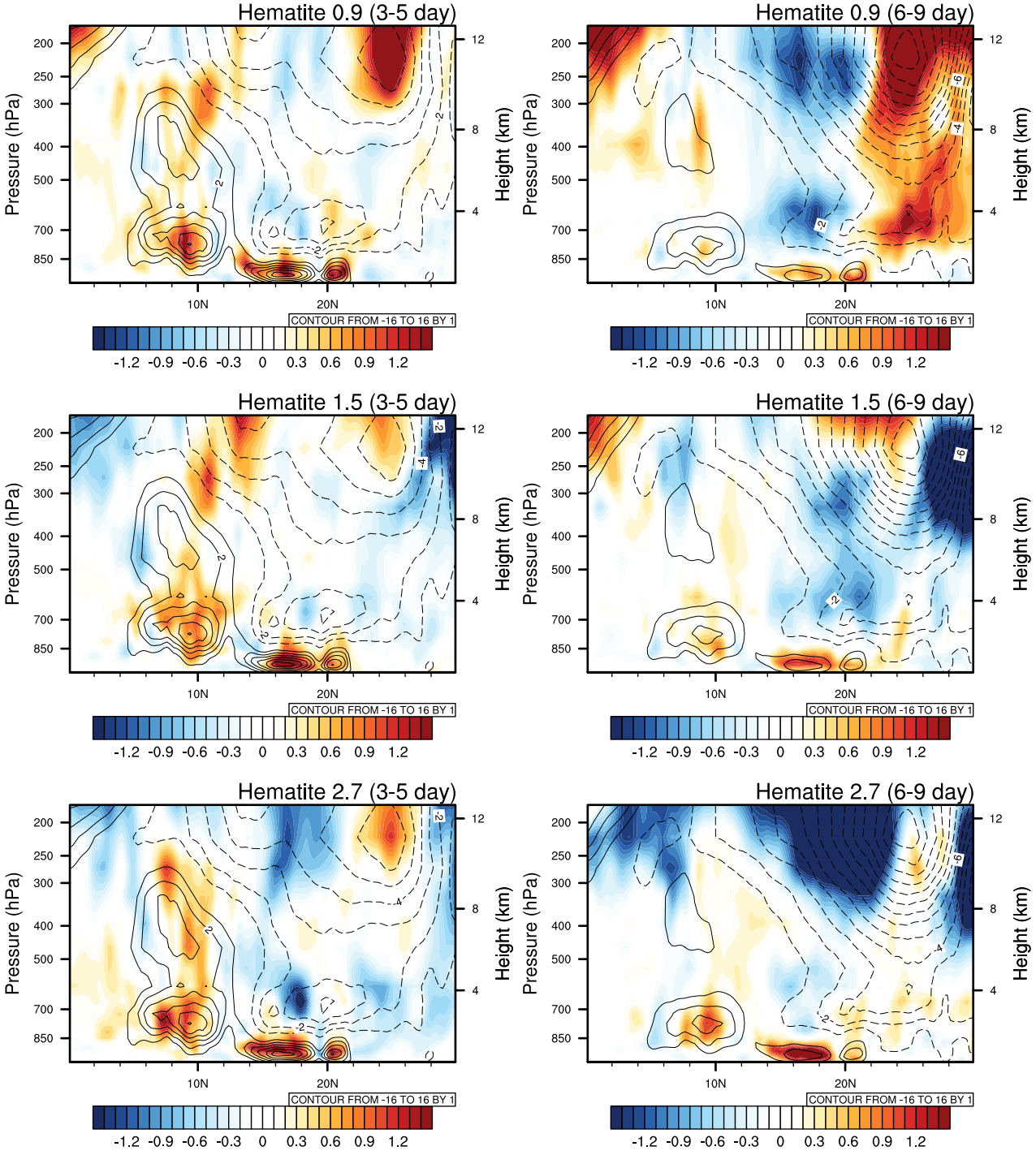
Hematite 0.9 (3-5 day)
Hematite 0.9 (6-9 day)
Hematite 1.5 (3-5 day)
Hematite 1.5 (6-9 day)
Hematite 2.7 (3-5 day)
Hematite 2.7 (6-9 day)
Pressure (hPa)
Height (km)
200
250
300
400
500
700
850
12
8
4
10N
20N
CONTOUR FROM -16 TO 16 BY 1
-1.2 -0.9 -0.6 -0.3 0 0.3 0.6 0.9 1.2

bpf_69_bias.png.

(a) Hematite0.9 - No Dust (6 - 9 days)

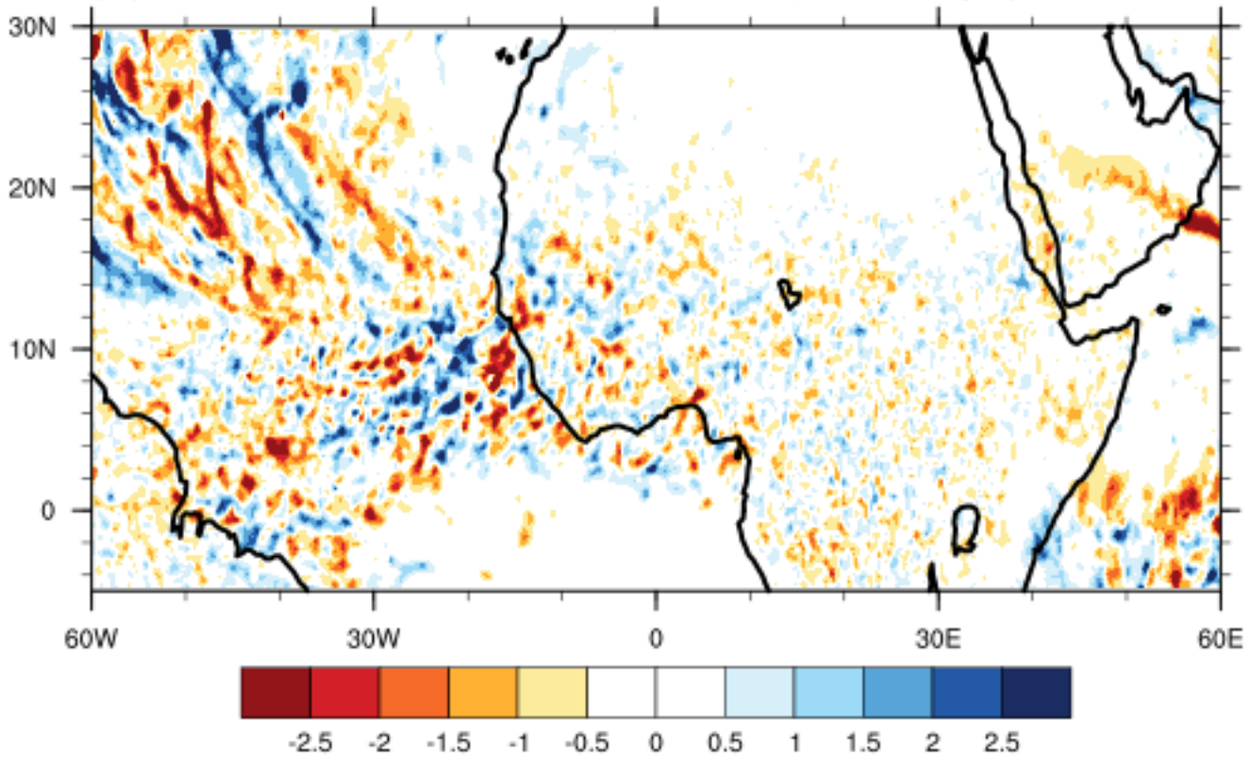

(b) Hematite1.5 - No Dust (6 - 9 days)

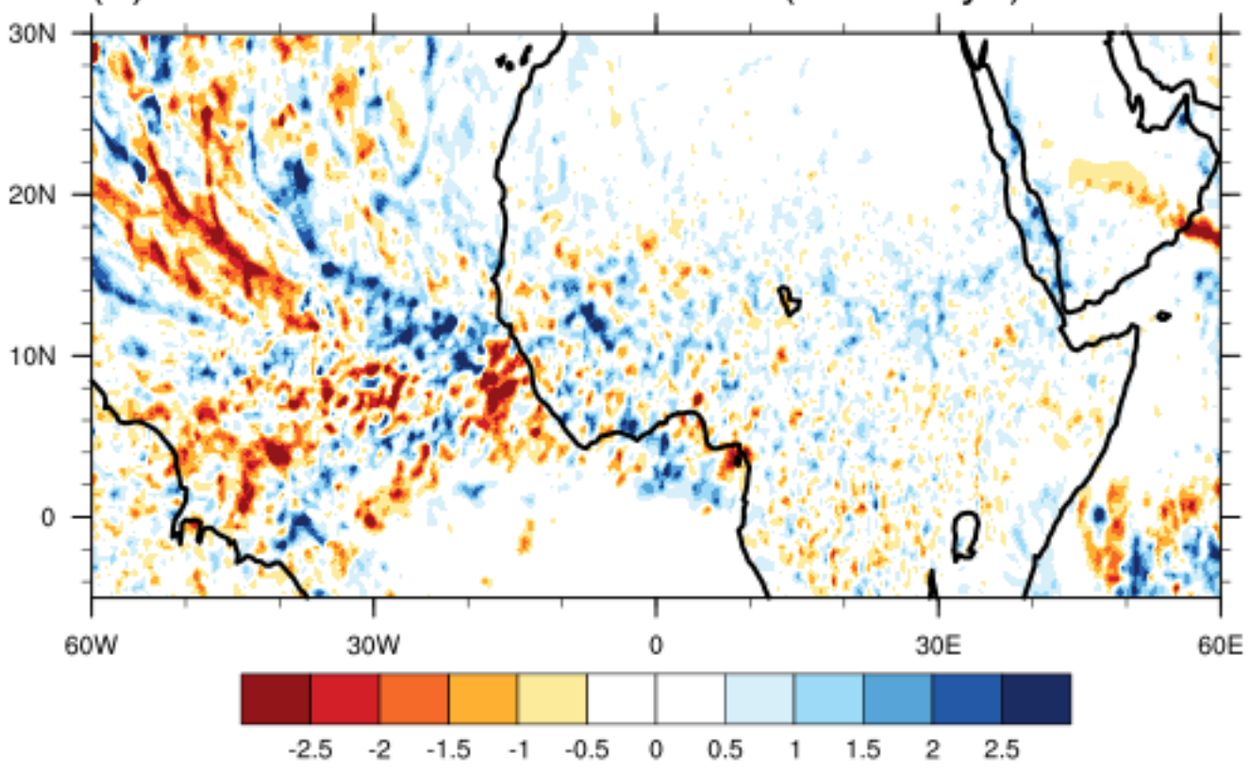

(c) Hematite2.7 - No Dust (6 - 9 days)

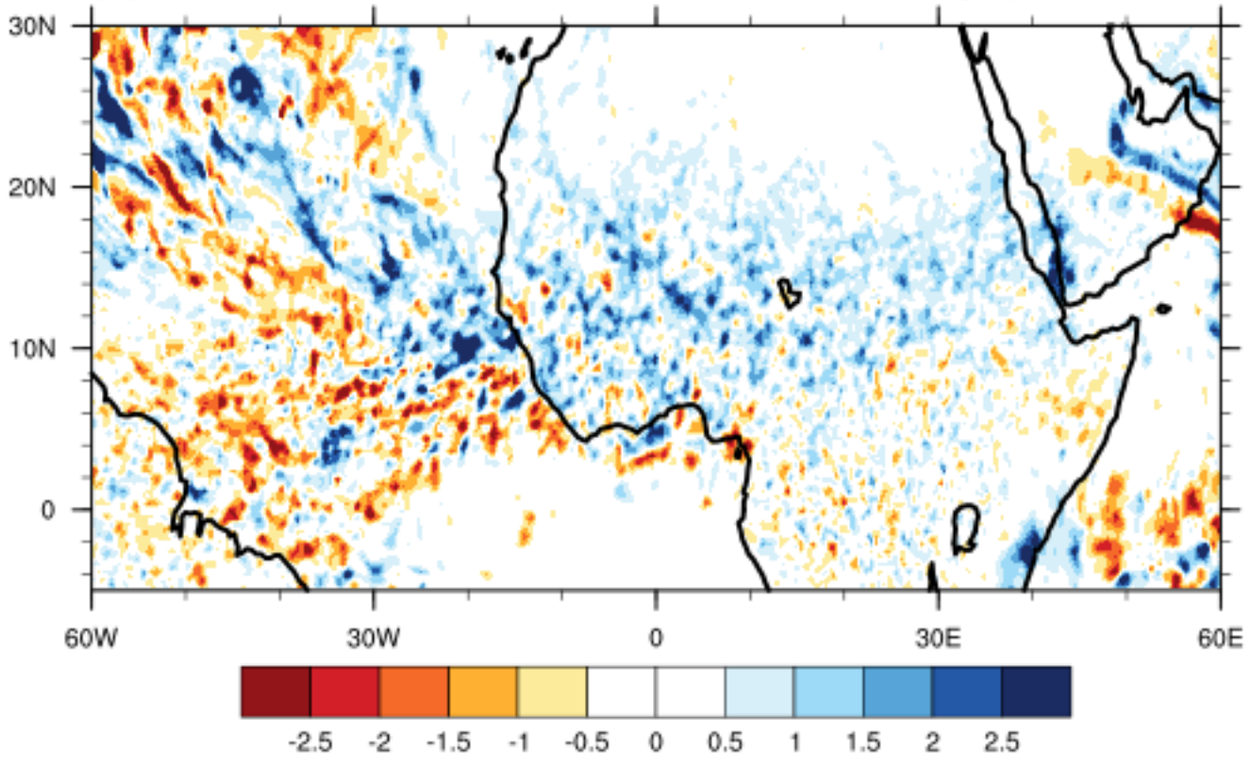

bpf_69_olr_bias.eps.

Hematite0.9 - No Dust (6 - 9 days)

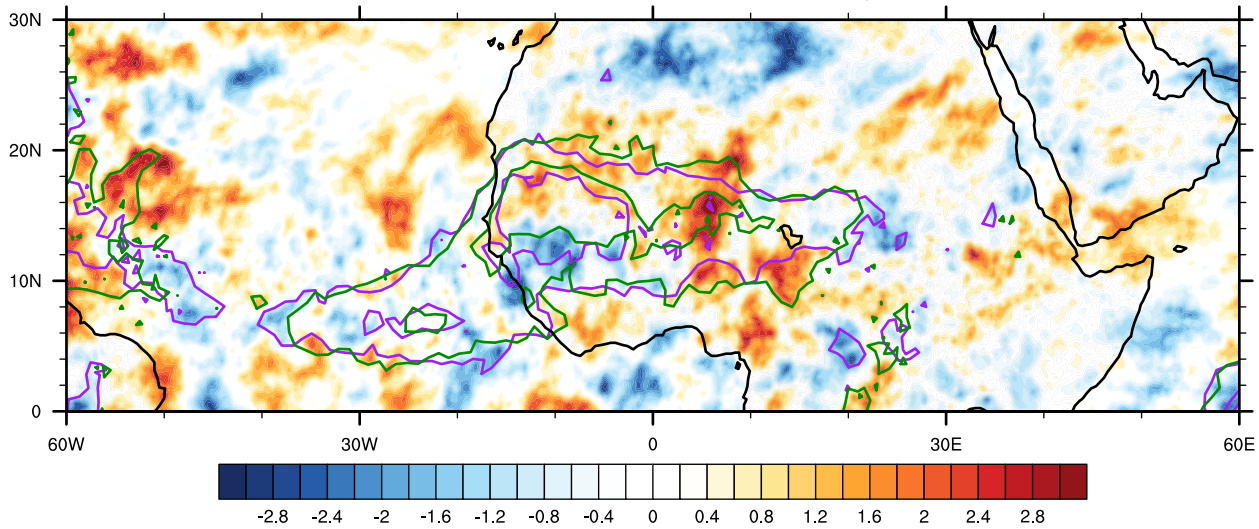

CONTOUR FROM 12 TO 18 BY 3

Hematite1.5 - No Dust (6 - 9 days)

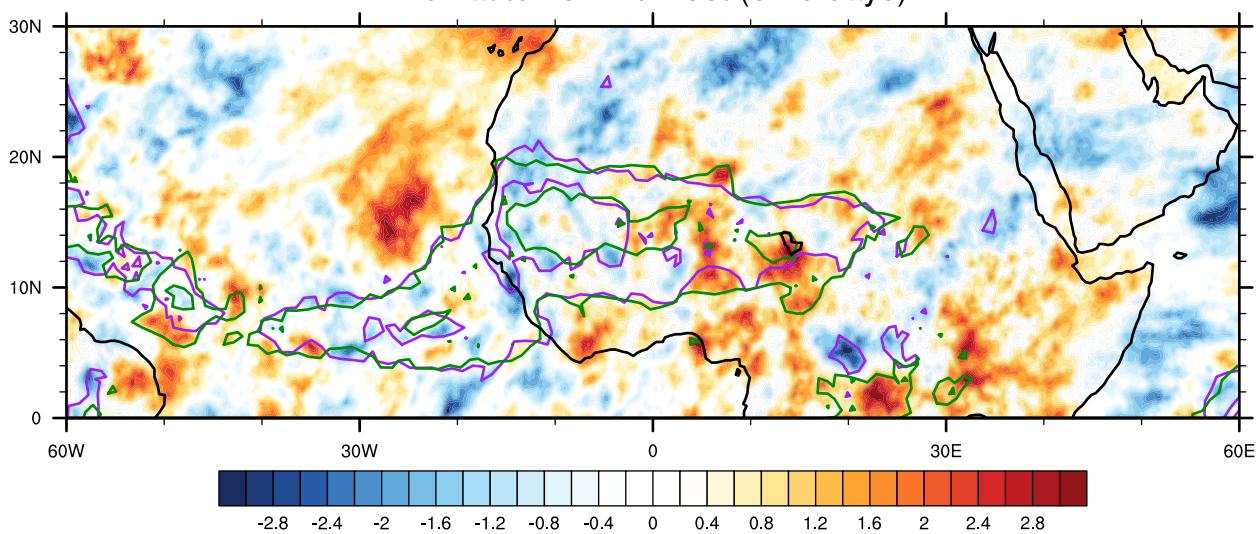

CONTOUR FROM 12 TO 18 BY 3

Hematite2.7 - No Dust (6 - 9 days)

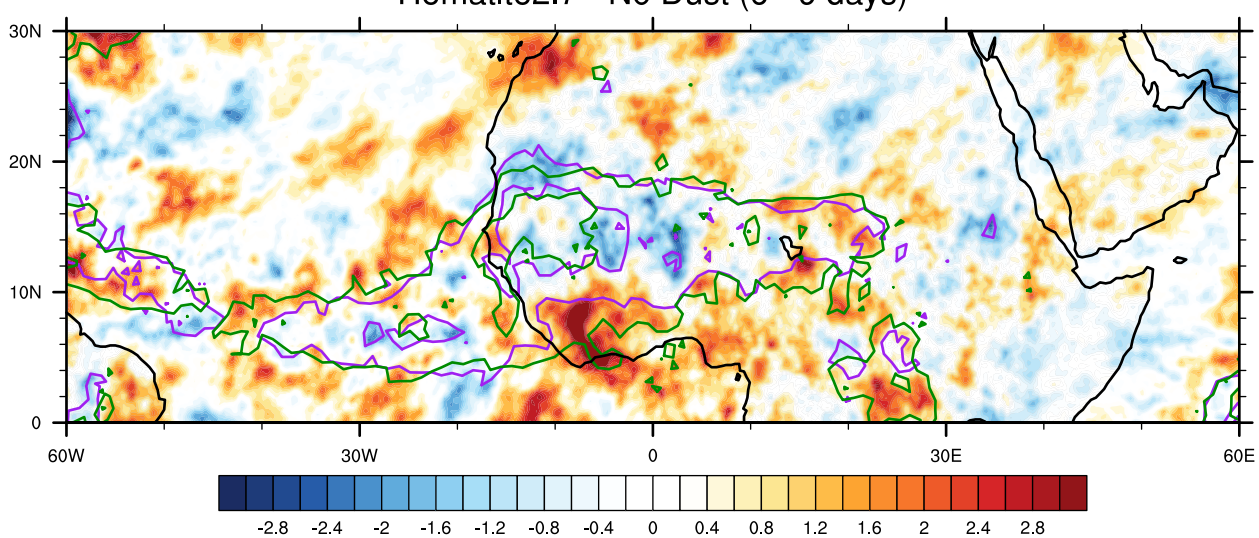

CONTOUR FROM 12 TO 18 BY 3

dh_ocean.eps.

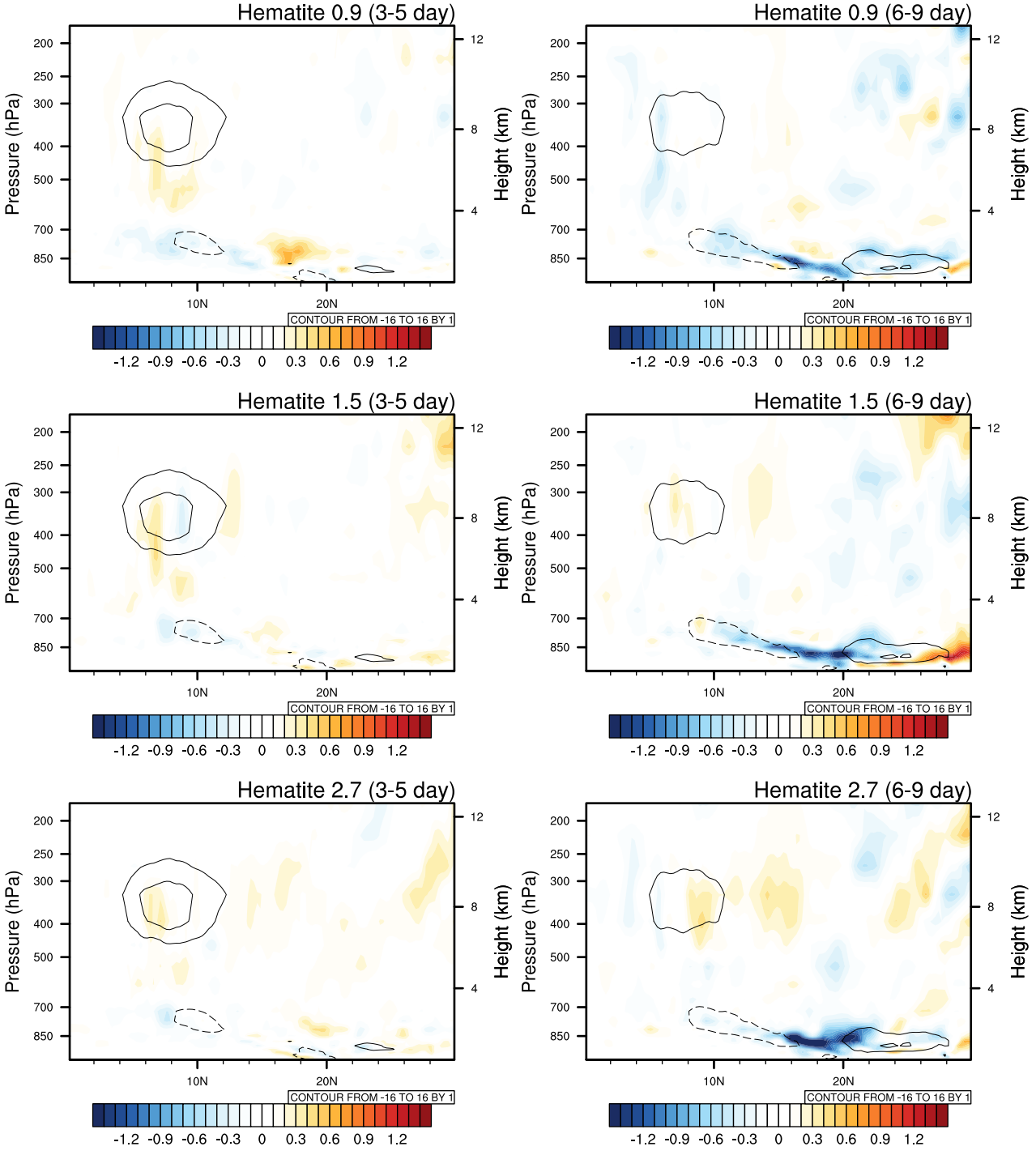
Hematite 0.9 (3-5 day)
Hematite 0.9 (6-9 day)
Hematite 1.5 (3-5 day)
Hematite 1.5 (6-9 day)
Hematite 2.7 (3-5 day)
Hematite 2.7 (6-9 day)
Pressure (hPa)
Height (km)
200
250
300
400
500
700
850
12
8
4
10N
20N
CONTOUR FROM -16 TO 16 BY 1
-1.2 -0.9 -0.6 -0.3 0 0.3 0.6 0.9 1.2

bt_land.eps.

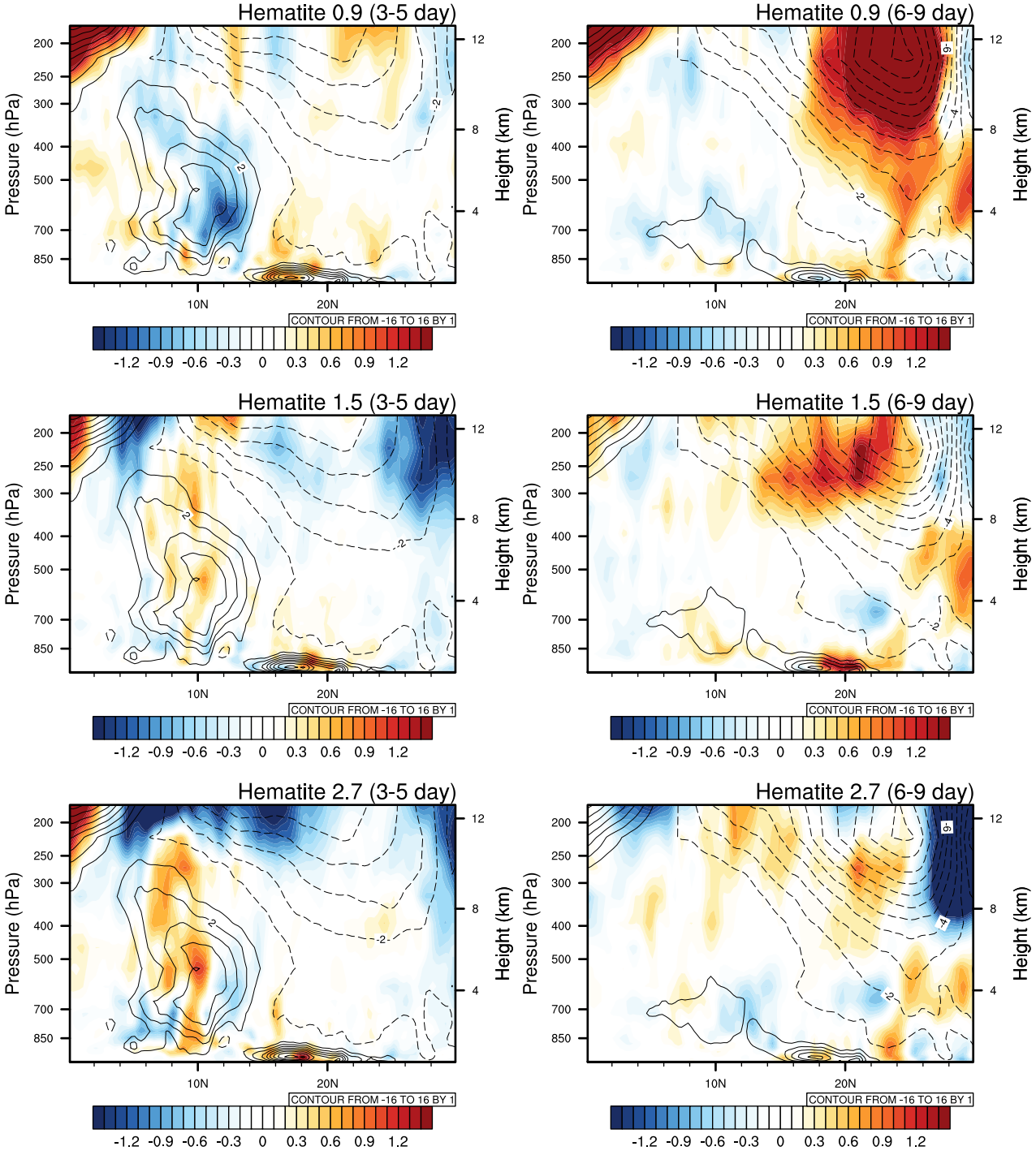
Hematite 0.9 (3-5 day)
Hematite 0.9 (6-9 day)
Hematite 1.5 (3-5 day)
Hematite 1.5 (6-9 day)
Hematite 2.7 (3-5 day)
Hematite 2.7 (6-9 day)
Pressure (hPa)
Height (km)
200
250
300
400
500
700
850
12
8
4
10N
20N
CONTOUR FROM -16 TO 16 BY 1
-1.2 -0.9 -0.6 -0.3 0 0.3 0.6 0.9 1.2

dh_land.eps.

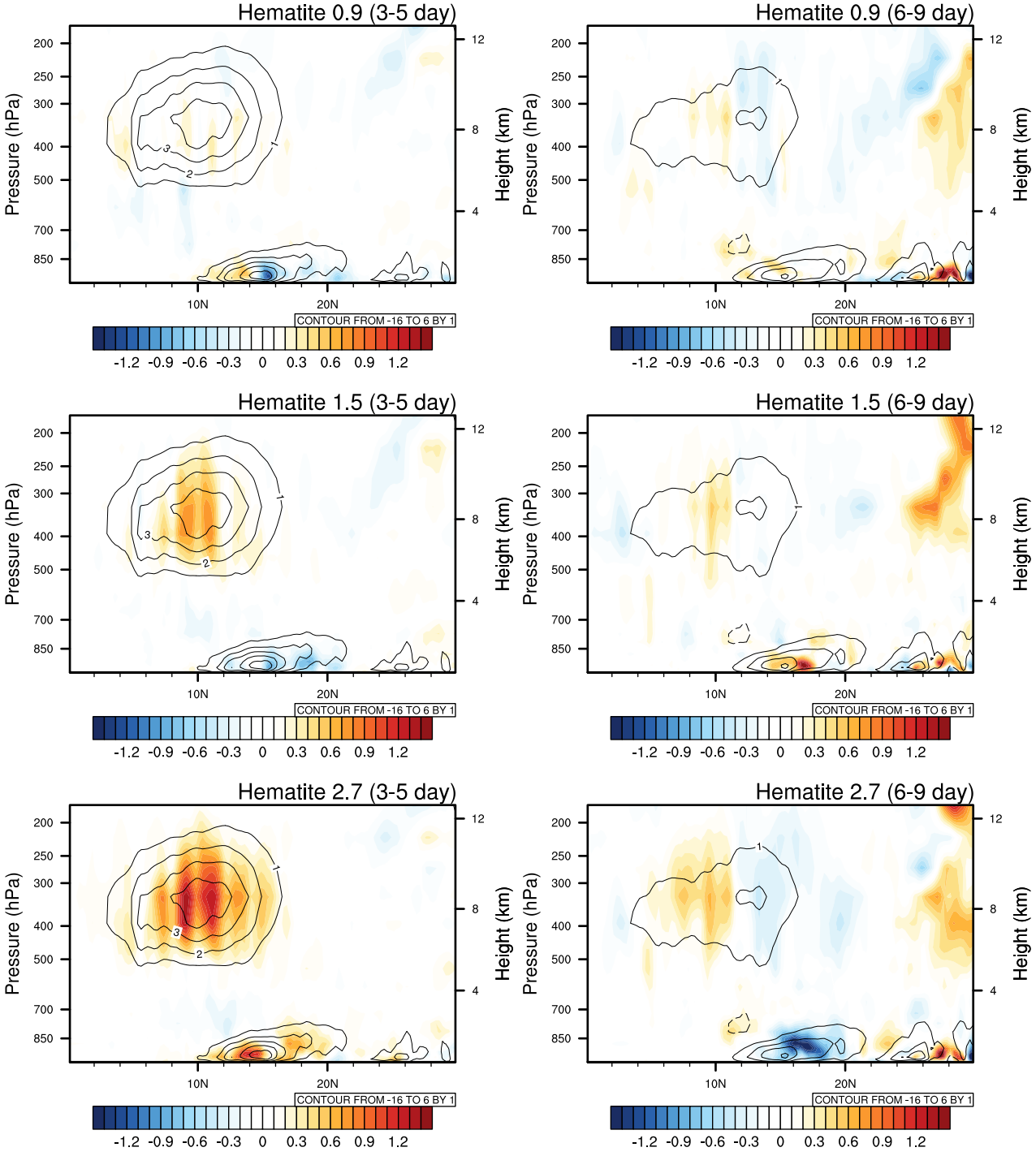
Hematite 0.9 (3-5 day)
Hematite 0.9 (6-9 day)
Hematite 1.5 (3-5 day)
Hematite 1.5 (6-9 day)
Hematite 2.7 (3-5 day)
Hematite 2.7 (6-9 day)
Pressure (hPa)
Height (km)
200
250
300
400
500
700
850
12
8
4
10N
20N
CONTOUR FROM -16 TO 6 BY 1
-1.2 -0.9 -0.6 -0.3 0 0.3 0.6 0.9 1.2

mape_land.eps.

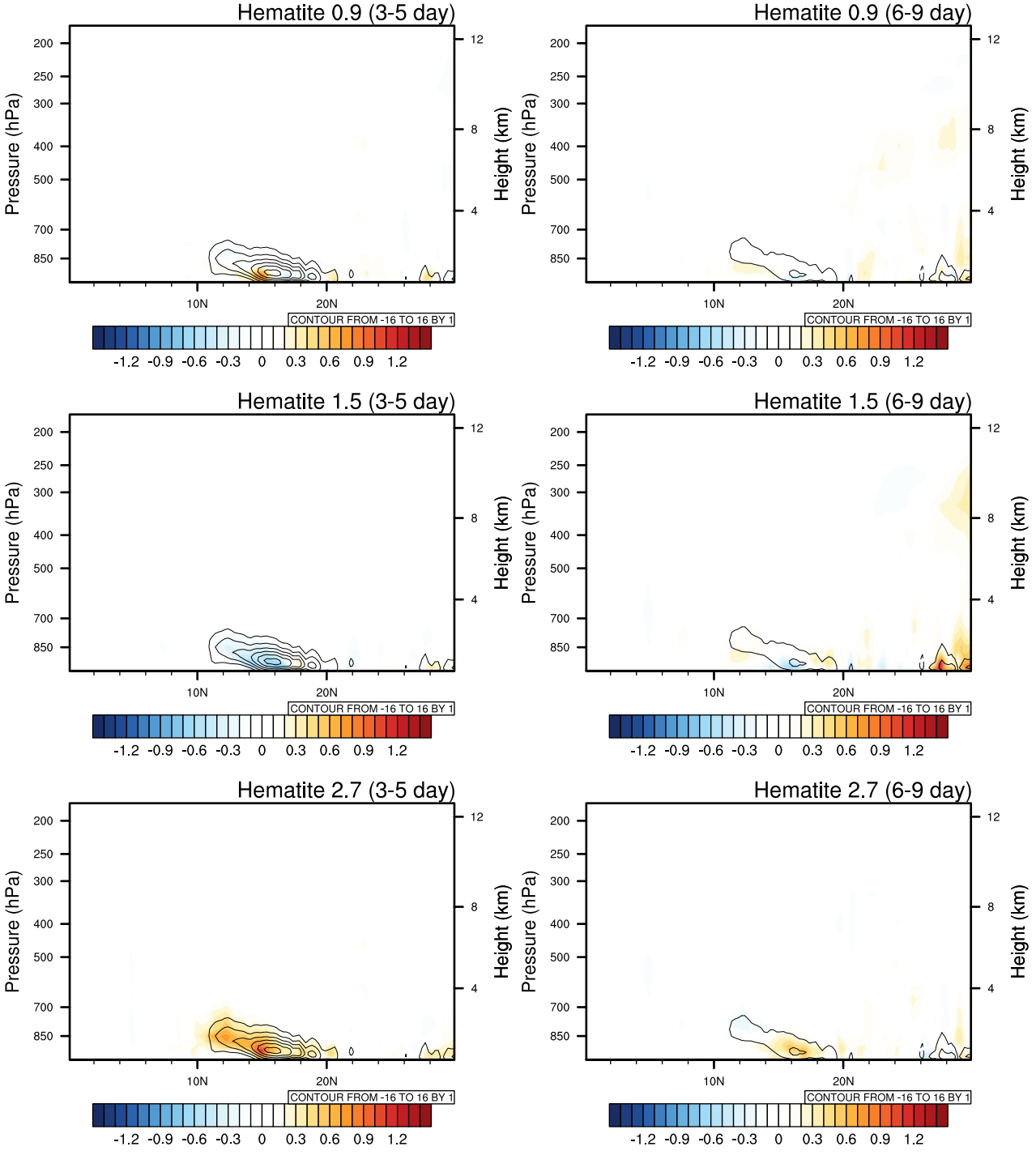
Hematite 0.9 (3-5 day)
Hematite 0.9 (6-9 day)
Hematite 1.5 (3-5 day)
Hematite 1.5 (6-9 day)
Hematite 2.7 (3-5 day)
Hematite 2.7 (6-9 day)
Pressure (hPa)
Height (km)
200
250
300
400
500
700
850
12
8
4
10N
20N
CONTOUR FROM -16 TO 16 BY 1
-1.2 -0.9 -0.6 -0.3 0 0.3 0.6 0.9 1.2

mape_ocean.eps.

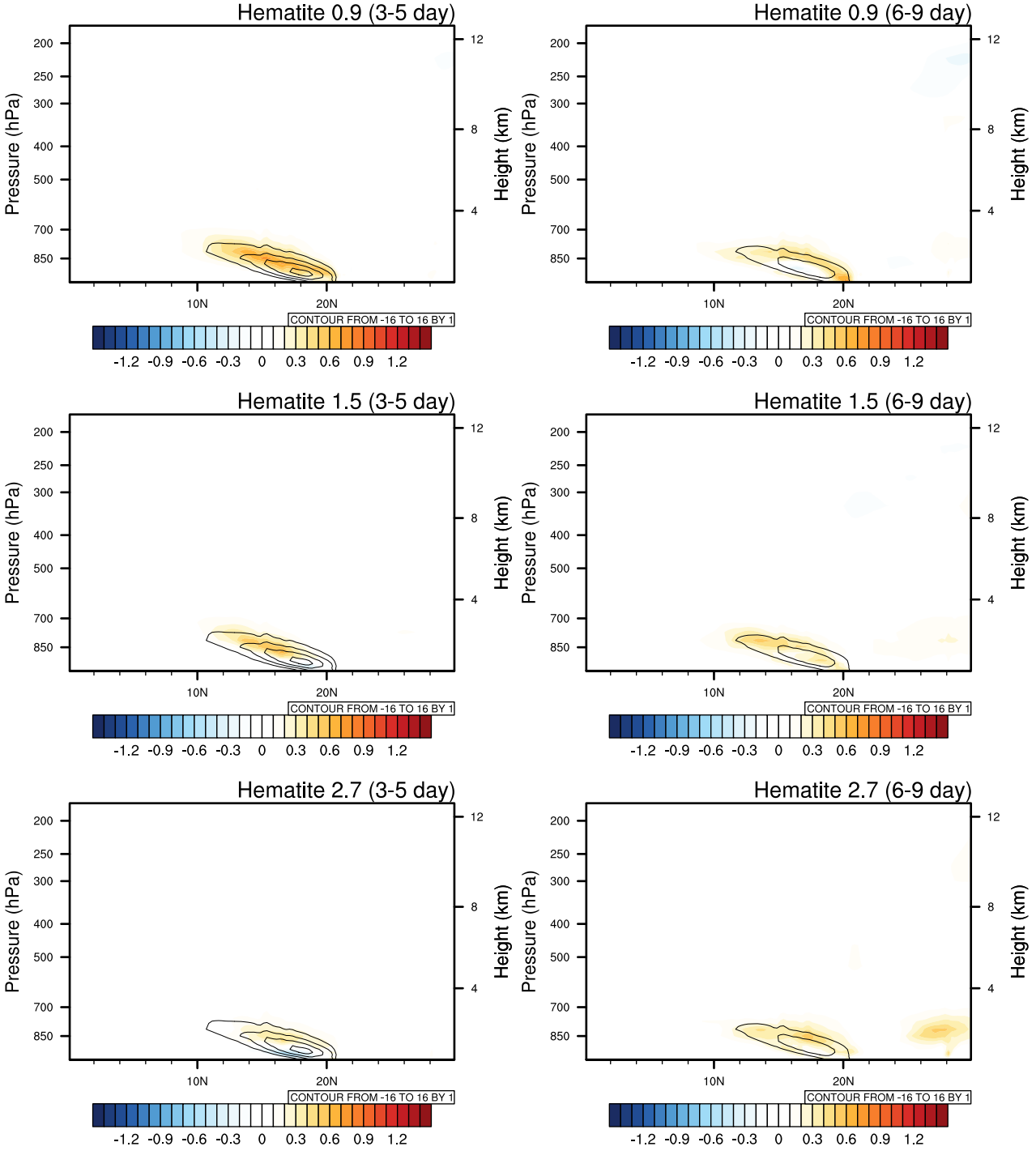
Hematite 0.9 (3-5 day)
Hematite 0.9 (6-9 day)
Hematite 1.5 (3-5 day)
Hematite 1.5 (6-9 day)
Hematite 2.7 (3-5 day)
Hematite 2.7 (6-9 day)
Pressure (hPa)
200
250
300
400
500
700
850
Height (km)
12
8
4
10N
20N
CONTOUR FROM -16 TO 16 BY 1
-1.2 -0.9 -0.6 -0.3 0 0.3 0.6 0.9 1.2

eke_35_bias_700.png.

Hematite0.9 - No Dust (3 - 5 days)

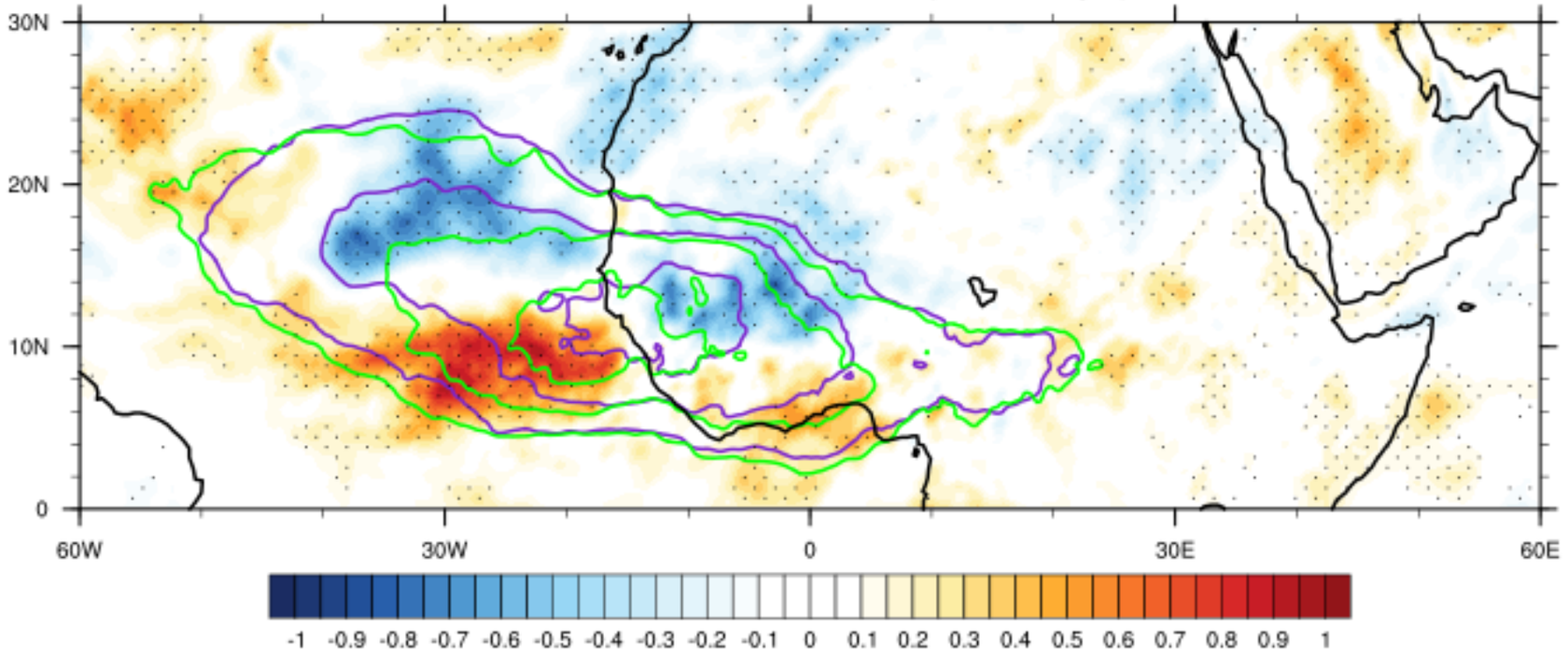

CONTOUR FROM 3 TO 7 BY 1

Hematite1.5 - NoDust (3 - 5 days)

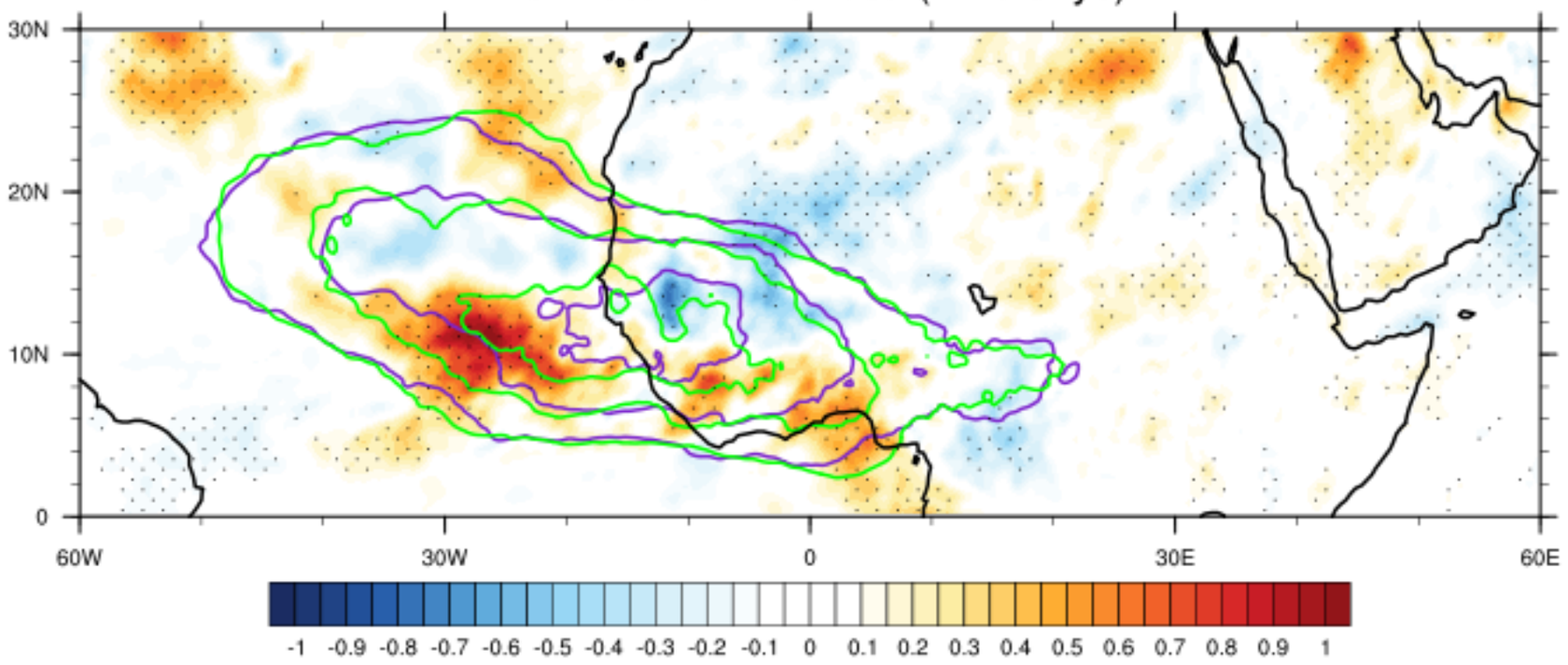

CONTOUR FROM 3 TO 7 BY 1

Hematite2.7 - No Dust (3 - 5 days)

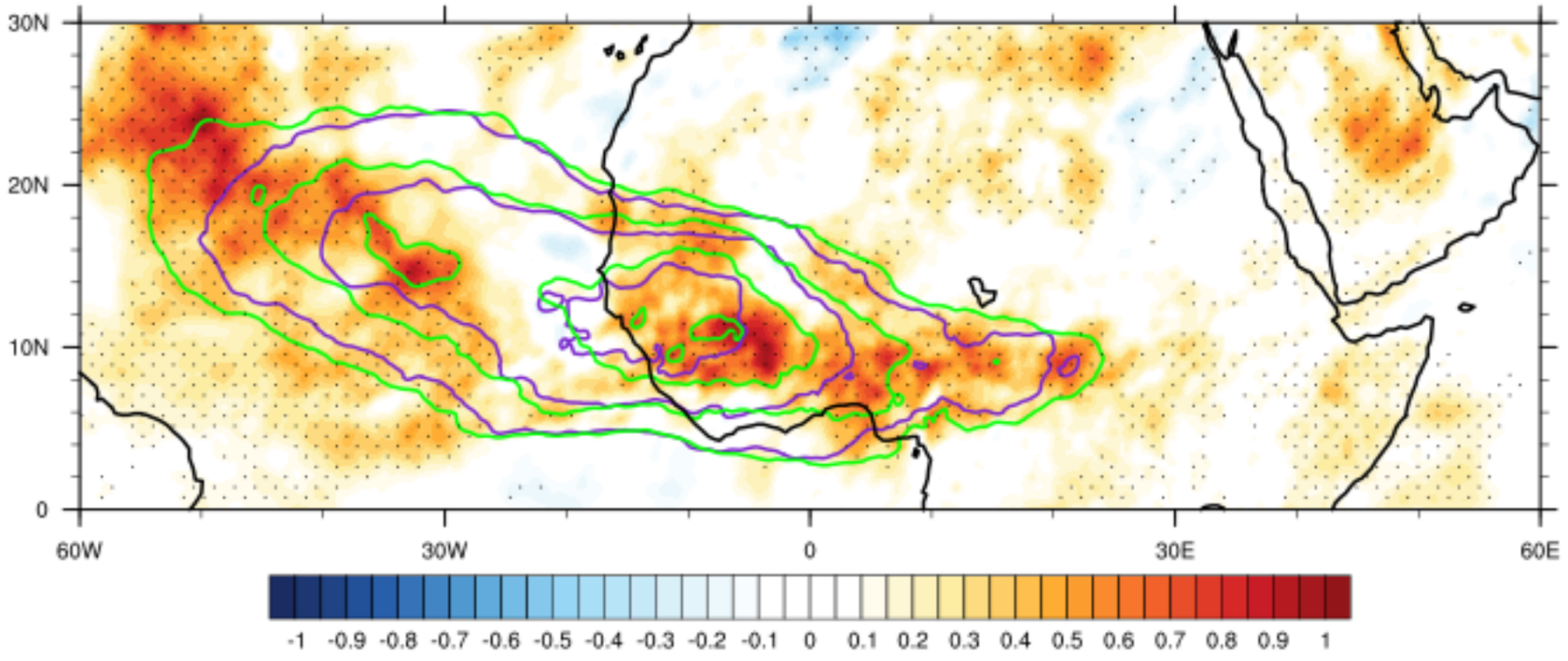

CONTOUR FROM 3 TO 7 BY 1

eke_69_bias_700.png.

Hematite0.9 - No Dust (6 - 9 days)

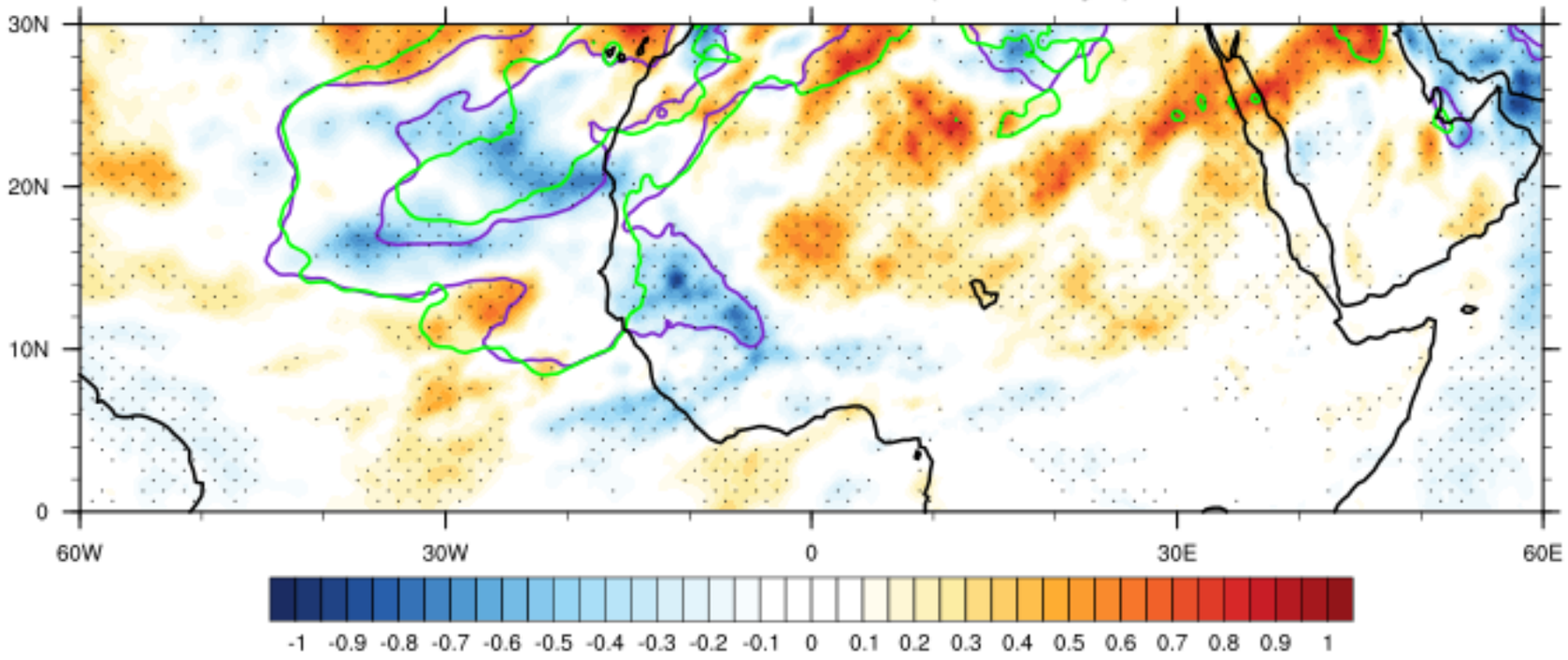

CONTOUR FROM 3 TO 7 BY 1

Hematite1.5 - NoDust (6 - 9 days)

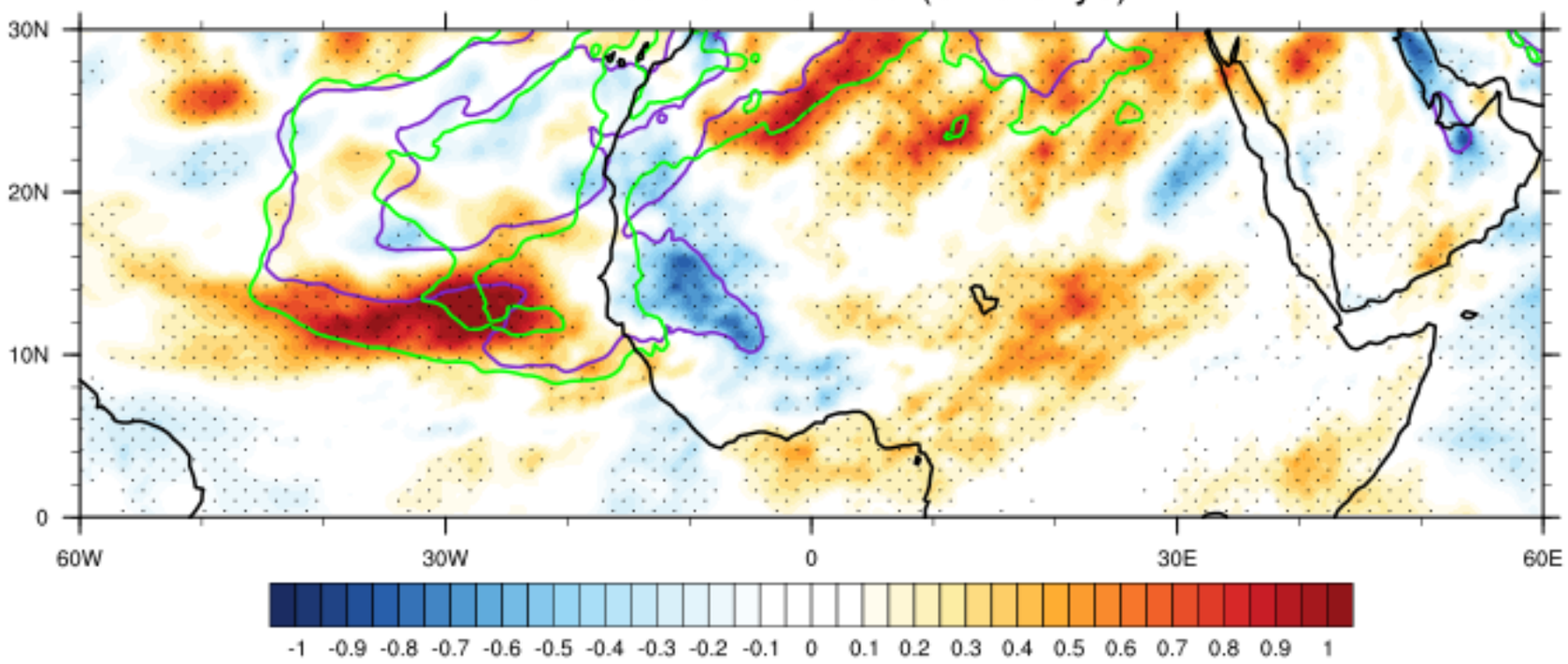

CONTOUR FROM 3 TO 7 BY 1

Hematite2.7 - No Dust (6 - 9 days)

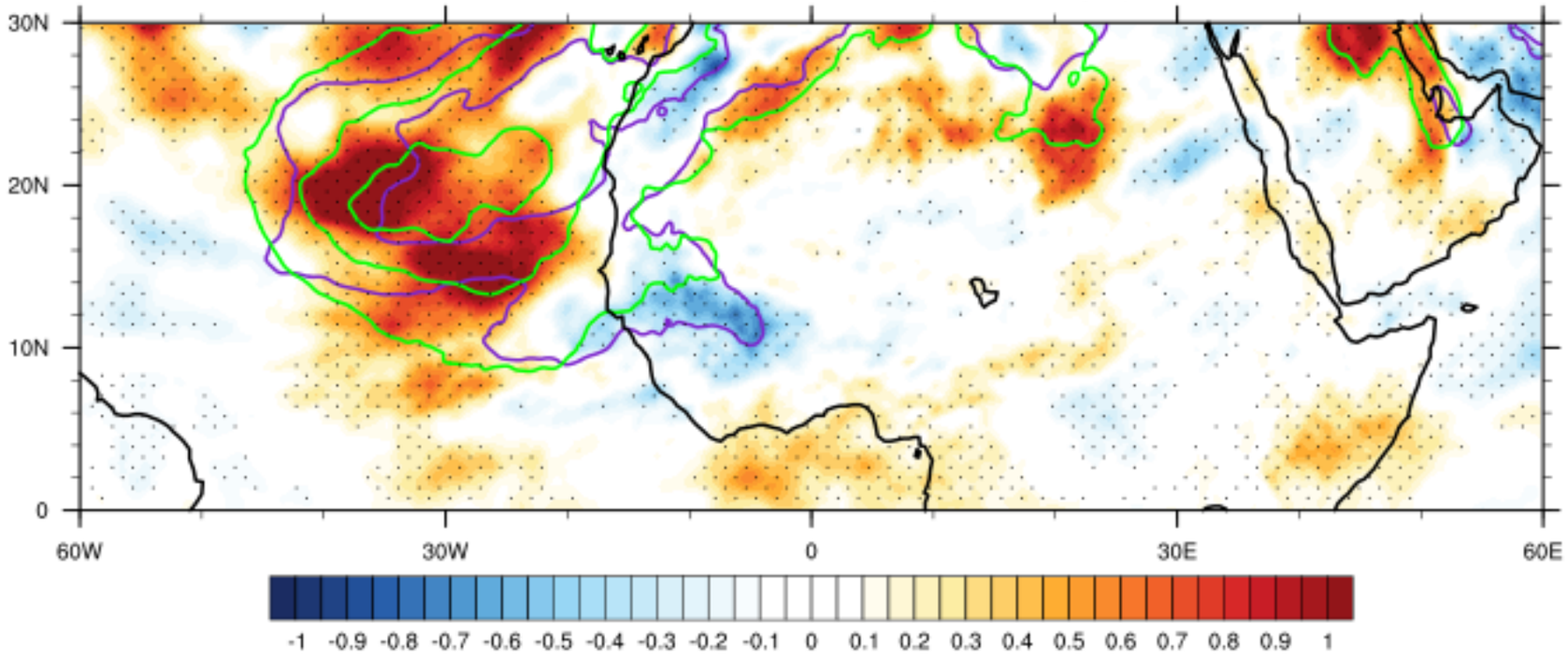

CONTOUR FROM 3 TO 7 BY 1